The role of subduction and gravitational sinking in particle export, carbon sequestration, and the remineralization length scale in the California Current Ecosystem

Michael R. Stukel [1,2]* Hajoon Song,[3] Ralf Goericke,[4] Arthur J. Miller[4]

[1]Department of Earth, Ocean, and Atmospheric Science, Florida State University, Tallahassee, Florida
[2]Center for Ocean-Atmospheric Prediction Studies, Florida State University, Tallahassee, Florida
[3]Massachusetts Institute of Technology, Cambridge, Massachusetts
[4]Scripps Institution of Oceanography, University of California at San Diego, La Jolla, California

Abstract

Particles and aggregates created in the surface layers of the ocean are transported not only by gravity, but also by the horizontal and vertical advection of the surrounding water. Subduction, in particular, can transport organic matter from the surface ocean to the mesopelagic in a manner that is not likely to be detected by typical in situ carbon export measurements (e.g., sediment traps and ^{238}U-^{234}Th disequilibrium). To assess the importance of subduction to the biological pump, we combined in situ sediment trap, thorium, primary productivity, and particulate organic carbon (POC) measurements with a data-assimilative physical circulation model and a Lagrangian particle tracking model. We develop a simple parameterization of two alternative particle sinking processes (Phytoplankton-Fecal Pellet [PFP] and Aggregation) using results from 13 extensively sampled water parcels in the California Current Ecosystem. Both parameterizations suggested that subduction is an important, at times dominant, mechanism of POC vertical export in the region (median 44% and 23% contribution to total POC export for PFP and Aggregate parameterizations at the 100-m depth horizon). The percentage contribution of subduction was highly variable across water parcels (ranging from 7% to 90%), with subduction typically more important in offshore, oligotrophic regions. On average the fate of particles that are passively transported out of the surface layer by advection is different from that of particles that sink across the 100-m depth horizon. Subducted particles were predominantly remineralized shallower than 150 m, while approximately 50% of gravitationally exported POC was remineralized at depths > 500 m.

The biological carbon pump (BCP) refers to a suite of processes that transport organic carbon fixed by phytoplankton in the surface ocean into the deep ocean, thus leading to sequestration of atmospheric carbon dioxide (CO_2) (Ducklow et al. 2001). The BCP includes diverse mechanisms of carbon transport including the gravitational settling of particles and aggregates, active transport of matter by vertically-migrating organisms, and passive transport of dissolved and particulate organic matter (DOM and POM, respectively) by physical advection or diffusion. The role of subduction in transporting inorganic and organic carbon to depth has long been qualitatively understood but has not often been quantified (Volk and Hoffert 1985). Indeed, the first large-scale manipulative experiment conducted to study the BCP in the open ocean was terminated when the Fe-enriched water parcel was subducted beneath the surface (Law et al. 1998; Stanton et al. 1998). Nevertheless, most BCP research has focused on the sinking of particles, a process which is amenable to in situ quantification (e.g., by sediment traps and radionuclide disequilibrium techniques) and was assumed to be the dominant component of the BCP (Ducklow et al. 2001; De La Rocha and Passow 2007; Honjo et al. 2008).

Overall, mass balance requires that the sum of the processes comprising the BCP, when expressed as fluxes of nitrogen, must balance the introduction of nitrogen into the ecosystem (Eppley and Peterson 1979). However, new production and net community production measurements typically exceed contemporaneous measurements of gravitational flux made with sediment traps or ^{234}Th (Bacon et al. 1996; Maiti et al. 2009; Estapa et al. 2015; Stukel et al.

*Correspondence: mstukel@fsu.edu

2015). Similarly, global estimates of export flux derived from *f*-ratio calculations (new production/primary production) are consistently higher than those based on *e*-ratio calculations (gravitational flux/primary production) (Dunne et al. 2005; Henson et al. 2011; Laws et al. 2011) and estimates of meso-pelagic respiratory demand exceed the supply of carbon from sinking particles (Burd et al. 2010). Taken together, this evidence suggests that other mechanisms of export (subduction, vertical mixing, and/or active transport) may be important components of the BCP.

The roles of vertical mixing and subduction (hereafter referred to together as passive export) in organic carbon flux have been difficult to determine from in situ data. Geochemical tracer approaches (e.g., apparent oxygen utilization or seasonal changes in nutrient stocks) implicitly combine passive export and gravitational particle flux (e.g., Takahashi et al. 1985; Goes et al. 2000; Sarmiento et al. 2002; Schlitzer 2002). Time-series measurements of dissolved organic carbon (DOC) inventories can be used to estimate passive transport of DOM (Carlson and Ducklow 1995), however such approaches cannot differentiate passive export from gravitational flux for particles. Instead, direct measurements of passive particle export require in situ measurement of three-dimensional POM fields in combination with the determination of physical currents and diffusivity (typically derived from a circulation model). The sampling intensity and multiple disciplines required for such studies have limited their use to date. Hence, relatively few studies have simultaneously quantified passive POM export and gravitational flux in this manner. Omand et al. (2015) used autonomous measurements coupled with a process-study ocean model and found that eddy-driven subduction may be responsible for up to half of particulate organic carbon (POC) export during the North Atlantic spring bloom. Stukel et al. (2017) used extensive sampling of a mesoscale front and vertical velocities derived from a circulation model to determine that subduction was similarly responsible for approximately half of the POC export in the frontal region.

In contrast, numerous researchers have studied passive export using models, either by combining region- to global-scale gridded DOM fields with general circulation models or by embedding biogeochemical models in general circulation models. Such studies typically find that subduction from the euphotic zone (EZ) is responsible for $\sim$ 20–50% of total organic matter export (Plattner et al. 2005; Najjar et al. 2007; Karleskind et al. 2011; Levy et al. 2013). Both modeling approaches have limitations: Large-scale gridded fields blur important seasonal and mesoscale variations in standing stocks. Biogeochemical models often oversimplify sinking as a process (e.g., a single sinking speed for all sinking particles), lack appropriate data necessary for parameterization of transfer functions (Franks 2009), and often lack export measurements that could be used for validation. An alternate approach is to use a particle tracking model parameterized
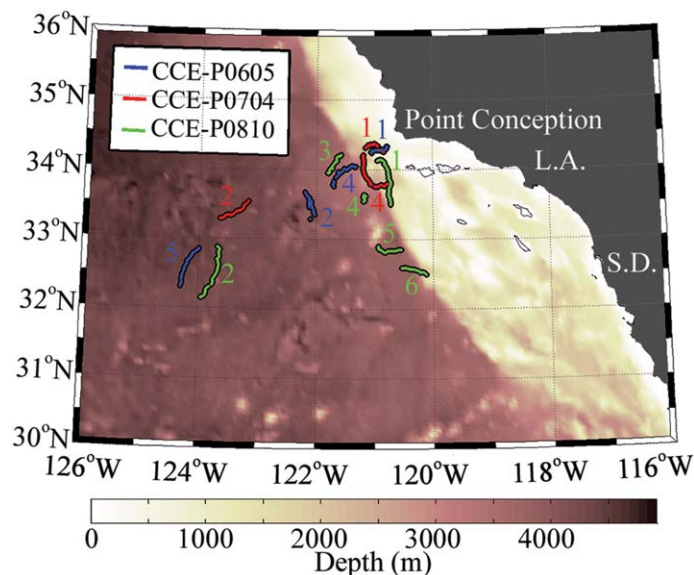

Fig. 1. Lagrangian cycle locations (blue, red, and green lines for P0605, P0704, and P0810 cruises, respectively) in the CCE with bathymetry map.

using in situ conditions to simultaneously quantify sinking and subducted POC. In the past, such approaches have been applied to assess horizontal, rather than vertical, transport (Siegel and Deuser 1997; Siegel et al. 2008).

The ability of geochemical tracer approaches (and in situ new and net community production methods) to measure the sum of all export terms may make it appealing to ignore the difference between gravitational flux and passive export. However, these two processes may lead to substantially different fates for exported carbon with respect to depth of remineralization, sequestration time scale, and utilization by different components of the ecosystem. For instance, while gravitational flux typically attenuates with depth following an exponential decay or power law decrease (Martin et al. 1987; Boyd and Trull 2007; Buesseler et al. 2007), Kahler et al. (2010) found that DOC subduction out of the surface layer of the subtropical North Atlantic was substantial, but that little of it penetrated deeper than 95 m.

The California Current Ecosystem (CCE, Fig. 1) is an eastern boundary current biome that includes high productivity coastal upwelling regions, intermediate productivity regions with wind-stress curl driven upwelling, and offshore oligotrophic regions that are linked to the coastal/shelf regions by Ekman transport and mesoscale processes (Lynn and Simpson 1987; Gruber et al. 2011; Ohman et al. 2013). To understand the relative contributions of gravitational and passive particle export and the fate of this exported material, we combined in situ gravitational flux and POC concentration measurements from three process cruises of the CCE long-term ecological research (LTER) program with a data-assimilating physical model fit to cruise conditions and a

Lagrangian particle tracking model. This approach allowed us to constrain the vertical motions of particles that sink (with a wide range of sinking speeds) as they are advected through the ocean. We found that the contribution of subduction to total vertical POC transport varied substantially, ranging from 7% to 90% and averaging $\sim$ 25–40%, depending on the model used. Furthermore, we determined that the remineralization length scale is substantially longer for particles transported primarily by gravitational export than for particles transported primarily by subduction, suggesting that gravitational flux leads to a longer carbon sequestration time scale than subduction.

Model description

Particle sinking velocities

Biogeochemical models often assume that vertical carbon transport is mediated by the gravitational flux of sinking detritus, and that this detritus is comprised of a single or a few particle classes with fixed sinking speeds (e.g., Fasham et al. 1990; Chai et al. 2002; Kishi et al. 2007). In contrast, empirical studies show that marine detritus (i.e., nonliving POC) is a heterogeneous group of particles with varying shape, size, and density (Turner 2015). It is thus more appropriate to model particle sinking speed using a continuous distribution. Allometric and particle aggregation models have been developed that predict sinking speed as a function of particle size (e.g., Guidi et al. 2008; Burd and Jackson 2009). However, in situ measurements suggest that a particle's density has to be considered as well (McDonnell and Buesseler 2010). At the simplest level, we can classify particles based on sinking speed such that a particle of class i has a sinking speed S_i. Using this formulation, we can quantify the mass flux of particles with sinking speed S_i as:

$$\text{Flux}_i = S_i \times N_i \times M_{i,\text{ave}} \tag{1}$$

where N_i is the concentration of particles with a sinking speed S_i and $M_{i,\text{ave}}$ is the average mass of carbon in these particles (mg C particle^{-1}). We can then define the carbon standing stock of particles of class i, that has a sinking speed S_i as $C_i = N_i \times M_{i,\text{ave}}$ and calculate total carbon flux as:

$$\text{Flux}_{\text{total}} = \sum_{i=0}^{i=\infty} S_i \times C_i \tag{2}$$

The functional form of particulate biomass (C) as a function of particle sinking speed (S) is not known, but will be related to an (also unknown) function that relates particle production to particle sinking velocity. We will define this function as the particle production sinking spectrum (PP(S), Table 1). PP(S) thus describes the production rate of particles with various sinking speeds (note that particles include both living and nonliving material). The shape of PP(S) likely depends on many different ecological and chemical parameters including phytoplankton and zooplankton community

structure, nutrient availability, and aggregate stickiness. We will use two different parameterizations to approximate PP(S) under the assumption that the particle sinking spectrum is governed by aggregation processes or that it is composed of two discrete particle classes (modeled after phytoplankton and mesozooplankton fecal pellets). We will then use in situ measurements to objectively parameterize each model for PP(S) (Fig. 2).

For the aggregate (Agg) parameterization, we will assume that since particle concentration, sinking rate (i.e., removal rate), and carbon content all have a power law relationship with particle diameter (Alldredge and Gotschalk 1988; Jackson et al. 1997; Alldredge 1998), we can also model particle creation via a power law relation to size. It follows, therefore, that particle production will have a power law relationship to particle sinking velocity. Under these assumptions, PP(S) can be described as a function of the form:

$$\text{PP}_{\text{agg}}(S) = \alpha \times S^{\beta} \tag{3}$$

where α and β are parameters related to the specific ecological and chemical conditions experienced in situ and hence must be determined empirically.

For the phytoplankton-fecal pellet (PFP) parameterization, we will assume that PP(S) for either phytoplankton or fecal pellets can be described by a log-normal distribution. PP(S) for both particle types can then be described as:

$$\begin{aligned}
\text{PP}_{\text{PFP}}(S) = {} & \tau \frac{1-\Phi}{\sigma_1 \sqrt{2\pi} S} \exp\left(-\frac{(\ln(S)-\mu_1)^2}{2\sigma_1^2}\right) \\
& + \tau \frac{\Phi}{\sigma_2 \sqrt{2\pi} S} \exp\left(-\frac{(\ln(S)-\mu_2)^2}{2\sigma_2^2}\right)
\end{aligned} \tag{4}$$

where τ is the total particle production rate, Φ is the ratio of fecal pellet production to total particle production (measured in situ), and μ_1 and μ_2 are parameters related to the median sinking rate of phytoplankton and fecal pellets, respectively. As explained below, we can only objectively determine two parameters from Eq. 4 (in addition to Φ, which was measured experimentally) and hence must determine some parameters a priori. Rather than set the sinking rate for either phytoplankton or fecal pellets, we assume that the median sinking speed for fecal pellets is ψ times greater than the one for phytoplankton, thus, since the median of a log-normal distribution is equal to $\exp(\mu)$, $\mu_2 = \ln(\psi \exp(\mu_1))$. We will assume that fecal pellet sinking speeds are two orders of magnitude greater than phytoplankton and hence $\psi = 100$. This value for ψ was chosen based on many studies that have shown sinking speeds for individual phytoplankters to be on the order of 1 m d^{-1} (e.g., Smayda and Bienfang 1983), while mesozooplankton fecal pellet sinking velocities are on the order of 100 m d^{-1} (Turner 2002). For simplicity, we also assume that the coefficient of variation for sinking

Table 1. Model parameters. "measured" means that values were calculated for each cycle from in situ measurements (Table 3).

Parameter	Units	Value	Explanation
S	m d^{-1}		Sinking speed
PP(S)	mg C m^{-2} d^{-1}/(m d^{-1})	Function	Particle production as a function of sinking speed. PP(S) integrated over all sinking speeds is equal to total primary production
Flux(z, S)	mg C m^{-2} d^{-1}/(m d^{-1})	Function	Sinking flux of particles with a sinking velocity S at a depth z. The integral of Flux(z, S) with respect to sinking speed has units of mg C m^{-2} d^{-1}.
C(z, S)	mg C m^{-3}/(m d^{-1})	Function	Concentration of particles with a sinking velocity S at a depth z. The integral of C(z, S) with respect to sinking speed has units of mg C m^{-3}.
λ	d^{-1}	measured	Remineralization rate
d_{prod}	m	measured	Mean depth of particle production (calculated from in situ ^{14}CPP profiles for each cycle).
Agg parameterization			
α	mg C m^{-2} d^{-1}/(m d^{-1})	measured	Related to the intercept (in log-log space) of the particle production to sinking speed relationship
β	dimensionless	measured	Related to the slope (in log-log space) of the particle production to sinking speed relationship
PFP parameterization			
τ	mg C m^{-2} d^{-1}	measured	Total particle production rate
μ_1	dimensionless	measured	Related to the median sinking rate of phytoplankton (e$^{\mu 1}$ = median sinking rate)
Ψ	dimensionless	100*	Ratio of median sinking speed of fecal pellets to median sinking speed of phytoplankton
σ_1, σ_2	dimensionless	1*	Standard deviation of the natural logarithm of PP(S), also called the scale or shape parameter
μ_2	dimensionless	ln (Ψe$^{\mu 1}$)	Related to the median sinking rate of phytoplankton (e$^{\mu 2}$ = median sinking rate)
Φ	dimensionless	measured	Ratio of fecal pellet production to total particle production (determined from in situ grazing measurements)

*The value of 100 for Ψ was chosen by comparing sinking speeds of phytoplankton and fecal pellets in Fig. 2 of Stukel et al. (2014). A value of 1 was chosen a priori for the scale parameter (σ_1 and σ_2), because it gave reasonable sinking speed distributions (a mode value with relatively low sinking rates, but a long tail of higher sinking rates).

speeds of the two particle types is equal (hence $\sigma_1 = \sigma_2$) and assume that $\sigma = 1$. While this is a subjective choice for σ, it generates particle sinking speed distributions that reflect reasonable expectations for sinking speed variability for these two particle classes. We have also tested the sensitivity of the model to different a priori parameterizations of σ (0.5 or 2.0) and found relatively small differences in model output (< 10% change to model mean values). Our simple assumptions about σ and ψ leave us with only two unknown parameters (μ_1 and τ) that can now be objectively determined using in situ measurements.

Note, the PFP parameterization does not include dynamic transformation of phytoplankton to fecal pellets, but rather assumes that particles are created in the EZ with sinking speeds corresponding to either phytoplankton or fecal pellets. The log-normal distribution used for the PFP parameterization was chosen for two reasons. First, it is consistent with our basic understanding of particle sinking speeds in the ocean (slowly sinking particles are more common than rapidly sinking particles, although rare rapidly sinking particles such as salp fecal pellets or large diatom aggregates certainly exist, Smayda 1971; Bienfang 1980). Second, it provides a distinctly different shape for PP(S) than the power-law distribution used for the Agg parameterization. While there are other equations that could be used to describe two populations that have different mean sinking speeds but for which the most common sinking speeds are concentrated toward the slower end of the spectrum, the use of a power-law distribution for the Agg parameterization and a double log-normal for the PFP parameterization served our goal of testing the sensitivity of our modeling framework to starkly different assumptions about the shape of PP(S).

Our goal in using these two sinking distributions is not to suggest that one or the other is more accurate. Both are vast
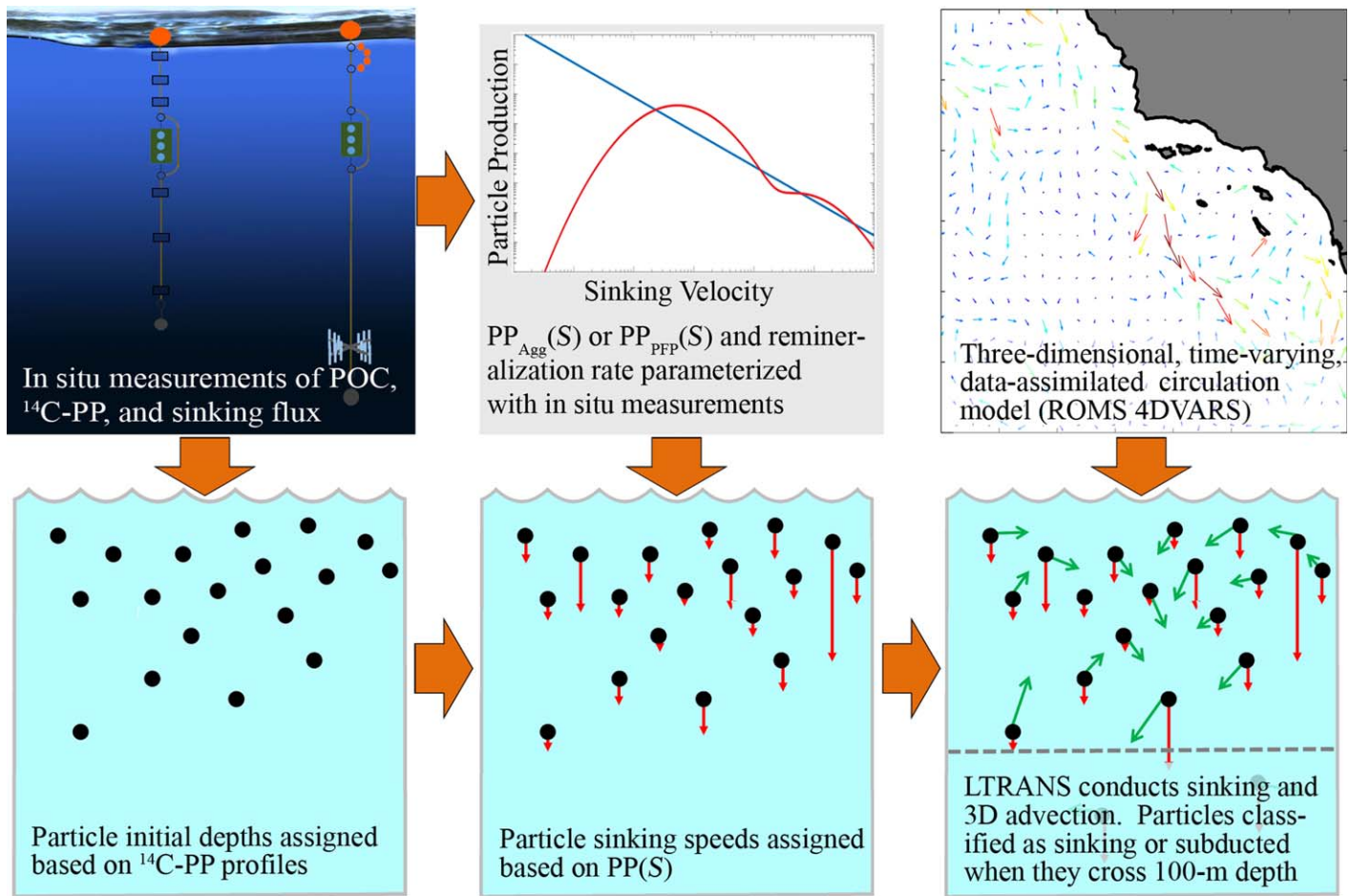
Fig. 2. Modeling approach conducted for both the Aggregate (Agg) and PFP parameterizations for each experimental cycle. In situ measurements are used to determine particle creation rates at different depths and the sinking rates of these particles (using either the Agg or PFP parameterizations). The 4DVARS circulation model (instantaneous surface fields are shown in upper right panel, but the model is four-dimensional) and particle sinking speeds are used by LTRANS to transport the particles in three dimensions.

oversimplifications of the complex processes of particle formation and degradation. Rather, we want to test the sensitivity of our results to parameterizations that encapsulate the different assumptions arising from two common, but fundamentally different, viewpoints about the processes driving particle sinking velocities. The PFP parameterization determines sinking speeds under the assumption that zooplankton fecal pellets are the dominant component of vertical flux due to high sinking speeds, despite the fact that they are less abundant than phytoplankton. The Agg parameterization assumes that aggregation processes drive particle sinking speeds and that both aggregate standing stock and sinking speed can be related to aggregate size by power laws. In situ particle sinking speed distributions likely involve a combination of these two processes that varies in space and time. We thus suggest that in situ sinking and subduction rates likely fall somewhere between the results we will find from the Agg and PFP parameterizations.

Parameterizing particle properties with in situ measurements

To define the parameters α and β in Eq. 3 or Φ, μ, and τ in Eq. 4, we used data from Lagrangian process studies conducted on three cruises in the CCE (Landry et al. 2009; Landry et al. 2012). These studies all sampled conditions that ranged from the coastal upwelling region near Point Conception to offshore waters characteristic of the California Current or oligotrophic subtropical gyre (Fig. 1; Table 2). Cruises were conducted in May 2006 (CCE-P0605), April 2007 (CCE-P0704), and October 2008 (CCE-P0810). On these cruises, water parcels were tracked for a period of 2–5 d using satellite-enabled drifters attached to 3x1-m holey-sock drogues centered at a depth of 15 m. Within these water parcels, primary productivity (^{14}CPP) was measured in polycarbonate bottles incubated in situ at six depths spanning the EZ (surface to 0.1% light level) using the $H^{14}CO_3^-$ uptake method (Stukel et al. 2011; Landry et al. 2012). POC

Table 2. In situ data from Lagrangian cycles. Columns are: cycle name, date, sea surface temperature (degree C), sea surface chlorophyll (mg Chl a m^{-3}), primary productivity (mg C m^{-2} d^{-1}), vertically integrated POC (mg C m^{-2}), carbon export at the 100-m depth horizon (mg C m^{-2} d^{-1}), mean depth of primary productivity (d_{prod}, m), and depth of the deepest POC sample (d_{POC}, m). Mean ± standard deviation of the mean.

Cycle	Date	SST	SSChl	^{14}CPP	POC	Export	d_{prod}	d_{POC}
0605-1	11–15 May 2006	12	5.17	4170 ± 904	12,649 ± 1715	322 ± 200	6.4	51
0605-2	16–21 May 2006	15	0.11	539 ± 23	4777 ± 136	72 ± 44	31.9	101
0605-4	26–31 May 2006	15	0.89	1442 ± 126	5525 ± 368	132 ± 49	13.6	51
0605-5	01–05 Jun 2006	16	0.09	458 ± 76	4885 ± 331	76 ± 74	35.5	85
0704-1	04–08 Apr 2007	12	1.35	1215 ± 414	5296 ± 517	144 ± 13	11.3	55
0704-2	09–13 Apr 2007	14	0.22	573 ± 49	5248 ± 191	32 ± 6	30.2	99
0704-4	16–20 Apr 2007	12	0.99	2295 ± 458	6734 ± 319	121 ± 45	16.9	92
0810-1	04–08 Oct 2008	17	0.45	551 ± 90	5302 ± 638	74 ± 11	19.0	57
0810-2	09–14 Oct 2008	17	0.20	478 ± 15	4117 ± 219	69 ± 13	25.7	109
0810-3	15–18 Oct 2008	16	0.72	888 ± 45	5335 ± 112	78 ± 7	13.0	60
0810-4	19–21 Oct 2008	16	1.05	672 ± 60	9390 ± 768	149 ± 36	9.9	54
0810-5	22–24 Oct 2008	15	1.47	1670 ± 217	5597 ± 188	127 ± 22	8.8	53
0810-6	25–28 Oct 2008	17	0.22	316 ± 29	3219 ± 280	107 ± 5	22.5	68

concentration was measured at eight depths in the EZ by filtering 1–2 L of seawater through GF/F filters and analyzing the samples on a CHN analyzer at the Scripps Institution of Oceanography Analytical Facility (Samo et al. 2012; Stukel et al. 2012). Vertical particle flux was measured at a depth of 100 m (and on CCE-P0810 at depths of 50 m or 60 m when the EZ was shallow) using either ^{238}U-^{234}Th disequilibrium (CCE-P0605, Stukel et al. 2011) or VERTEX-style sediment traps that had been determined using ^{238}U-^{234}Th to be accurately collecting particles (Stukel et al. 2013).

We will define Flux(z, S) as equal to the carbon export of all particles with a given sinking speed (S) measured at a depth of z. To calculate parameters for Eqs. 3, 4, we make the simplifying assumptions that particle production is concentrated at a specific depth (d_{prod}, which we calculate from ^{14}CPP profiles below) and that particle remineralization (λ, units of d^{-1}) is independent of particle sinking speed or depth. Then, we can relate Flux(z, S) to PP(S) with the following equation:

$$\text{Flux}(z, S) = \text{PP}(S) \times e^{-\lambda(z - d_{prod})/S} \qquad (5)$$

Note that Eq. 5 is only defined for depths greater than d_{prod} and λ refers to all processes that remineralize POC to CO$_2$, including respiration by bacteria and zooplankton consumers. Then, PP(S), Flux(z, S), and d_{prod} can be related to parameters measured in situ by the following equations:

$$^{14}\text{CPP} = \int_{S=S_{min}}^{S=S_{max}} \text{PP}(S) dS \qquad (6)$$

$$\text{Export}_{z=100} = \int_{S=S_{min}}^{S=S_{max}} \text{Flux}(100, S) dS \qquad (7)$$

$$d_{prod} = \frac{\int z \times {}^{14}\text{CPP}(z) dz}{\int {}^{14}\text{CPP}(z) dz} \qquad (8)$$

From Eq. 2 above, we can relate the carbon content of all particles with a sinking speed S at a depth of z, C(z, S), to Flux(z, S) by the following equation:

$$\text{C}(z, S) = \frac{\text{Flux}(z, S)}{S} \qquad (9)$$

We can also relate C(z, S) to vertically integrated POC concentrations in the water column (POC$_{total}$) by the following equation:

$$\text{POC}_{total} = \int_{z=d_{prod}}^{z=d_{POC}} \int_S \text{C}(z, S) dS dz \qquad (10)$$

where d_{POC} is the maximum depth at which POC measurements are made (if shallower than the depth of the export measurement). Thus, we have four equations (Eqs. 6, 7, 8, 10) that are dependent on λ, d_{prod}, and PP(S) and hence if PP(S) is defined as a function that is dependent on only two undefined parameters (e.g., α and β for PP$_{agg}$ and μ_1 and τ for PP$_{PFP}$), we can use the above equations to solve for PP(S). The equations were solved in Matlab using a grid search approach while assuming that sinking speeds could vary from 1 mm d^{-1} (S_{min}) to 1 km d^{-1} (S_{max}).

Data-assimilating physical model

The three-dimensional physical model was implemented in the Regional Ocean Modeling System (ROMS) using the four-dimensional variational data assimilation system (4DVAR, Moore et al. 2011). The model had 9-km horizontal

resolution and 42 terrain-following vertical levels. The minimum thickness was less than 1 m near the surface along the coastal regions increasing up to 300 m near the bottom of the open ocean. 4DVAR updated the model initial condition and surface forcing to produce the dynamically-consistent four-dimensional estimate of the sea state that closely follows the observations over the 1 month period centered on each of our cruises. The initial and boundary conditions were derived from Broquet et al. (2009) for the 2006 and 2007 cruises, and the California Current System Reanalysis product by the University of California, Santa Cruz for the 2008 cruise. The surface forcing is from the 9-km resolution Coupled Ocean/ Atmosphere Mesoscale Prediction System (COAMPS, Hodur and Doyle 1999; Doyle et al. 2009). Assimilated observations included along-track sea surface height (Ssalto/Duacs) and sea surface temperature (AVHRR) and in situ temperature and salinity profiles collected by conductivity-temperature-depth (CTD) measurements on our cruises.

Data assimilation in 4DVAR computes the cost function, a measure of the distance between the model state and observations, and iteratively improves the model state to minimize it. Hence, the cost function is often used to represent the goodness of the data assimilation. The reductions by fitting the observations are 52%, 47%, and 55% for 2006, 2007, and 2008 cruises, respectively. For detailed information, readers are referred to Song et al. (2012) and Miller et al. (2015).

The 9-km horizontal resolution of the ROMS model is not fine enough to capture submesoscale circulation and hence may underestimate subduction rates. However, the importance of submesoscale dynamics to subduction in our region is uncertain. Omand et al. (2015) estimated that submesoscale eddy-driven vertical POC flux was proportional to squared mixed layer depth. Mixed layer depths in our study region (typically < 20–35 m) are substantially shallower than in high latitude regions such as the North Atlantic or Southern Ocean. We thus suspect that the increased horizontal resolution necessary to resolve the submesoscale would not substantially change our conclusions. However, since we cannot test this, our subduction rate estimates should be considered conservative.

To estimate trajectories of particles produced during the experimental cycles, we used a modified version of the Larval TRANSport Lagrangian model (LTRANS, North et al. 2006) that allowed individual sinking speeds for each particle as determined by Eqs. 3, 4. LTRANS advects and diffuses particles using the ROMS velocity and eddy diffusivity fields, while simultaneously sinking particles using sinking speeds derived from PP(S). For each cycle and parameterization (Agg and PFP), we released 10,000 particles that were generated at random locations along the drifter track of the cycle and depths proportional to the ^{14}CPP profiles, thus simulating the depth of particle creation. Particles were initialized with random sinking speeds derived from the particle production

as a function of sinking speed equations (Eq. 3 or Eq. 4) and remineralized with λ's calculated for each cycle. Crucially, all particles both sank and were subducted (or upwelled). However, we considered model particles to have been subducted if they crossed the 100-m depth horizon by advection and to have sunk (gravitationally) if they crossed the 100-m depth horizon by sinking (i.e., during the biological [sinking] or physical [advection] subroutines of LTRANS). We note that this operational definition is a stark dichotomy that does not exist in the ocean. However, in a statistical sense, it fits particle export that would be measured by sediment traps (e.g., if 75% of particles of a given speed were transported past a specific depth horizon by gravitational flux, we would expect 75% of these particles to be collected by a sediment trap at that depth horizon, assuming no hydrodynamic biases). In circumstances when physical advection caused a particle to cross the 100-m depth horizon multiple times, we determined sinking/subduction based on the final time that the particle crossed the depth horizon. Each particle was tracked for a total of 30 d.

Since many particles had not crossed the 100-m depth horizon within the 30 d data assimilated time frame (particularly for cycles that occurred near the end of a cruise), we extended the ROMS model for an additional month without fitting to observations, using the boundary conditions outlined above. As the boundary condition was extracted from the data assimilative ocean states, the ROMS model continuously received relatively accurate information from the boundary. While this second month of the ROMS model will have less well constrained currents, extending the simulation without data assimilation ensures smooth transition of currents for 2 months, which is desirable for our purpose. In addition, unassimilated currents have a much smaller impact on the results of our analysis, since most POC was remineralized within the first 30-d period (during which we had cruise data for assimilation).

Results

Modeled sinking distributions and in situ data

The in situ conditions sampled on these three cruises spanned a broad range of oceanic conditions (Table 2). Vertically integrated primary productivity varied from 316 mg C m^{-2} d^{-1} to 4170 mg C m^{-2} d^{-1}, while surface primary productivity varied from 7.5 mg C m^{-3} d^{-1} to 433 mg C m^{-3} d^{-1}. Similarly, surface chlorophyll a showed a wide range (0.09–5.2 mg Chl a m^{-3}). The dataset also included a range of ecosystem states with regards to bloom formation or decay. Different cycles featured conditions with protozoan grazing exceeding phytoplankton growth, mesozooplankton grazing exceeding phytoplankton growth, or phytoplankton growth substantially greater than the sum of the grazing terms (Landry et al. 2009).

Table 3. Model parameters (*see* Eqs. 3–5).

| Cycle	Aggregate			PFP				
	α	β	λ	τ	λ	$\exp(\mu_1)$	$\exp(\mu_2)$	Φ
0605-1	246	−1.16	0.30	4170	0.29	1.44	143.8	0.10
0605-2	32	−1.16	0.10	539	0.10	0.95	95.1	0.11
0605-4	86	−1.16	0.23	1442	0.21	2.80	280.1	0.06
0605-5	29	−1.14	0.08	458	0.07	1.43	143.3	0.05
0704-1	77	−1.13	0.20	1215	0.18	0.09	9.3	0.49
0704-2	24	−1.28	0.10	573	0.10	0.15	14.9	0.10
0704-4	117	−1.22	0.33	2295	0.33	0.14	14.3	0.23
0810-1	33	−1.15	0.09	551	0.08	1.68	167.6	0.03
0810-2	30	−1.14	0.10	478	0.10	1.64	164.3	0.08
0810-3	49	−1.19	0.15	888	0.15	0.63	62.5	0.11
0810-4	46	−1.09	0.05	672	0.04	1.72	171.6	0.05
0810-5	96	−1.17	0.27	1670	0.27	0.22	22.2	0.21
0810-6	23	−1.00	0.06	316	0.05	2.12	211.7	0.17

Fig. 3. (**a**) Probability density function of sinking speeds of particles as determined for Cycle 0605-1 using the Agg parameterization (blue) and the PFP parameterization (red). (**b**) Export flux as a function of particle sinking speed for Cycle 0605-1, calculated from Eq. 5 [same colors as (**a**)].

Using Eqs. 6, 7, 10, we solved for the parameters α, β, and λ for the Agg parameterization (Eq. 3). Despite the large variability in oceanic conditions, the parameter β (which quantifies the slope of the particle sinking speed spectrum) was relatively constant, varying from −1.28 to −1.00 (Table 3). The parameter α showed substantial variability (ranging from 23 to 246), as would be expected since it reflects the magnitude of particle creation at a sinking speed of 1 m d^{-1}, and hence covaries strongly with primary productivity. λ (the particle remineralization rate) was also quite variable, ranging from 0.06 d^{-1} to 0.33 d^{-1}. Particle creation was always dominated by the slowly sinking particles (since β was always negative). However, carbon export was dominated by faster sinking particles with sinking speeds > 10 m d^{-1} (Fig. 3 and Supporting Information Fig. 1). Cycle 0704-2 had the lowest mean sinking speed, with half of carbon export mediated by particles with a sinking speed slower than 46 m d^{-1}, while Cycle 0605-1 had the highest (half of export mediated by particles with a sinking speed > 150 m d^{-1}).

For the PFP parameterization, we calculated the ratio of fecal pellet production to total particle production (Φ) using in situ estimates of total phytoplankton production (^{14}C-method) and in situ estimates of mesozooplankton grazing derived from the gut pigment method (*see* Stukel et al. 2011; Stukel et al. 2013) combined with the assumption that mesozooplankton egestion efficiencies are $\sim 30\%$ (Conover 1966). From these calculations, we found that Φ ranged from 0.03 (during Cycle 0810-1 when grazing was dominated by protozoans) to 0.49 (Cycle 0704-1, which had high euphausiid abundance, Table 3). Median sinking speeds were highly variable for the PFP parameterization; 50% of export was mediated by particles with a sinking rate < 6 m d^{-1} for 0810-4, while 50% was mediated by particles with a sinking rate > 156 m d^{-1} for 0605-1. This variability in median
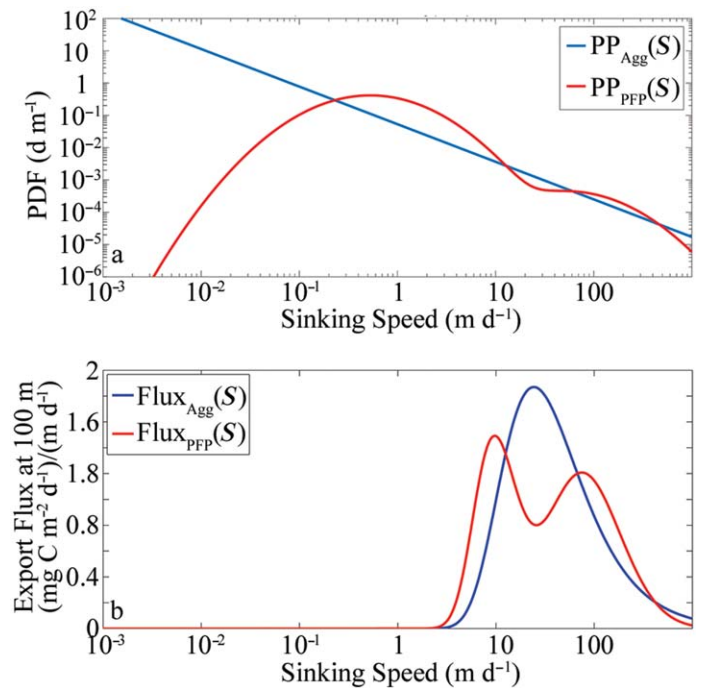
sinking rate was driven both by variability in the proportion of fecal pellets produced and by changes in the parameterized sinking rates of particles of each size class. Median fecal pellet sinking rates varied from 9 m d^{-1} to 280 m d^{-1}.

Three-dimensional particle advection and sinking models

We used a data assimilating ROMS model to track the three-dimensional transport of synthetic Lagrangian particles produced during each experimental cycle. Across the 13 cycles, the median net horizontal distance traveled by the particles over a 30-d period was 149 km. However, horizontal distance traveled was negatively correlated to particle sinking speed (negative correlation with $p \ll 0.01$ using Spearman's rank correlation for 25/26 cycle/parameterization combinations), both because surface currents were stronger than currents at depth and because the direction of the currents varied with depth. Compared to the long distances traveled by total particles, the mean (carbon-weighted) distance traveled by particles before they crossed the 100-m depth horizon was considerably shorter. For the PFP parameterization, mean horizontal POC transport prior to export across the 100-m depth horizon ranged from 9 km to 78 km for the 13 cycles (median = 26 km, mean = 34 km), while for the Agg parameterization it ranged from 5 km to 42 km (median = 15 km, mean = 19 km). This variability in distance traveled prior to export agrees with "the statistical funnel"
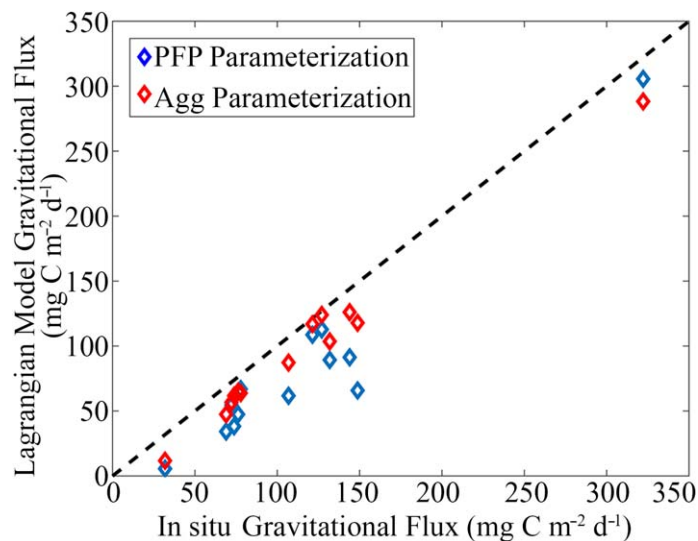
Fig. 4. Comparison of the Lagrangian particle modeling approach gravitational export measurements to in situ gravitational export measurements. Note that the Lagrangian particle approach predicts the eventual export of particles created during an experimental cycle, while the in situ measurements quantify export during the experimental cycle.

Fig. 5. Total vertical flux in the three-dimensional model with (**a**) the PFP parameterization and (**b**) the Agg parameterization. Blue is export by particles that gravitationally sank across the 100-m depth horizon and green is export by particles that were subducted across the 100-m depth horizon.

concept of theoretical sediment trap studies (Siegel et al. 1990; Siegel et al. 2008).

Gravitational flux estimates derived from both the PFP and Agg parameterizations showed strong correlation to in situ measurements, although the Lagrangian particle modeling approach estimates were consistently lower than the in situ observations (Fig. 4). This result is not surprising, since the in situ measurements explicitly determined export occurring *during* the occupation of each water parcel (or in the case of ^{234}Th : ^{238}U during and prior to occupation), while our modeling approach estimates the *eventual* export of particles *produced* during the occupation of the water parcel. In a coastal upwelling driven system, with a gradient of high productivity near the coast and low productivity onshore, and the aforementioned lateral advection of particles prior to export, we can expect particle export at the locations where particles sink to be lower than at the location where those same particles were formed. As an additional validation approach, we ran both parameterizations in a one-dimensional steady state configuration (i.e., lateral decoupling of production and export not allowed) and found that both parameterizations accurately estimated in situ carbon export and did a reasonable job recovering measured vertical profiles of POC (*see* Supporting Information Appendix and Supporting Information Figs. 2, 3).

To calculate the relative contribution of passive particle flux to carbon export, we quantified the percentage of particulate carbon that was transported across the 100-m depth horizon during the physical advection subroutine (as opposed to the gravitational sinking subroutine) of the
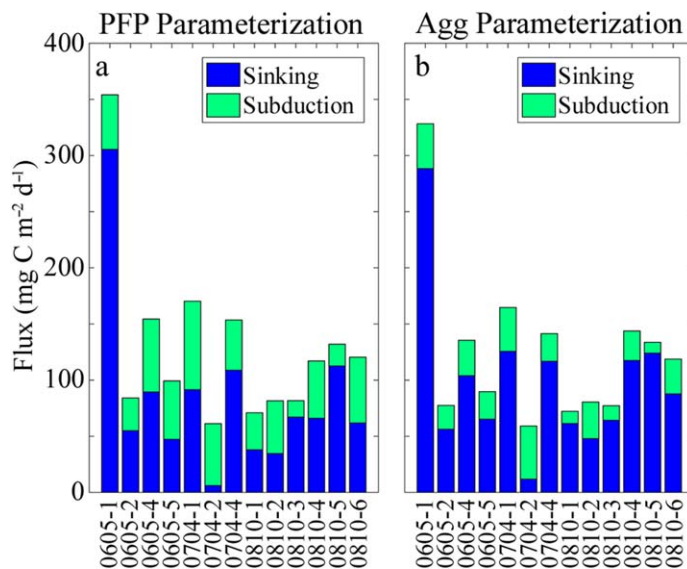
Table 4. Percentage contribution of subduction to total vertical carbon flux. Values in parentheses are the values determined by decreasing or increasing (respectively) the gravitational flux input to the model by one standard error.

	PFP	Agg
0605-1	13.7 (13.5–20.0)	12.2 (10.6–11.6)
0605-2	34.7 (32.1–40.9)	27.3 (31.3–25.6)
0605-4	42.1 (38.3–45.4)	23.3 (24.9–24.1)
0605-5	52.4 (53.1–85.3)	27.3 (38.6–25.5)
0704-1	46.3 (46.7–42.8)	23.7 (23.7–23.8)
0704-2	90.0 (91.5–85.2)	80.0 (80.3–75.4)
0704-4	29.1 (38.2–26.6)	17.4 (17.1–16.8)
0810-1	46.5 (45.3–47.3)	15.0 (15.6–13.9)
0810-2	57.7 (56.4–59.1)	40.5 (43.9–39.2)
0810-3	17.9 (18.8–15.4)	16.8 (16.9–15.1)
0810-4	43.6 (40.1–44.5)	18.3 (18.0–17.1)
0810-5	14.7 (17.5–13.3)	07.3 (09.8–08.4)
0810-6	48.7 (47.8–49.3)	26.1 (26.2–25.6)
Median	**43.6 (40.1–44.5)**	**23.3 (23.7–23.8)**

LTRANS model (Fig. 5a; Table 4). Hereafter, we will refer to these particles as subducted particles. For the PFP parameterization, results suggested that subduction contributed between 14% (Cycle 0605-1) and 90% (Cycle 0704-2) of total particulate export. The median and mean across all cycles were 44% and 41%, respectively. The contribution of passive flux was generally lower for cycles in more productive water parcels and was negatively correlated with τ (the particle
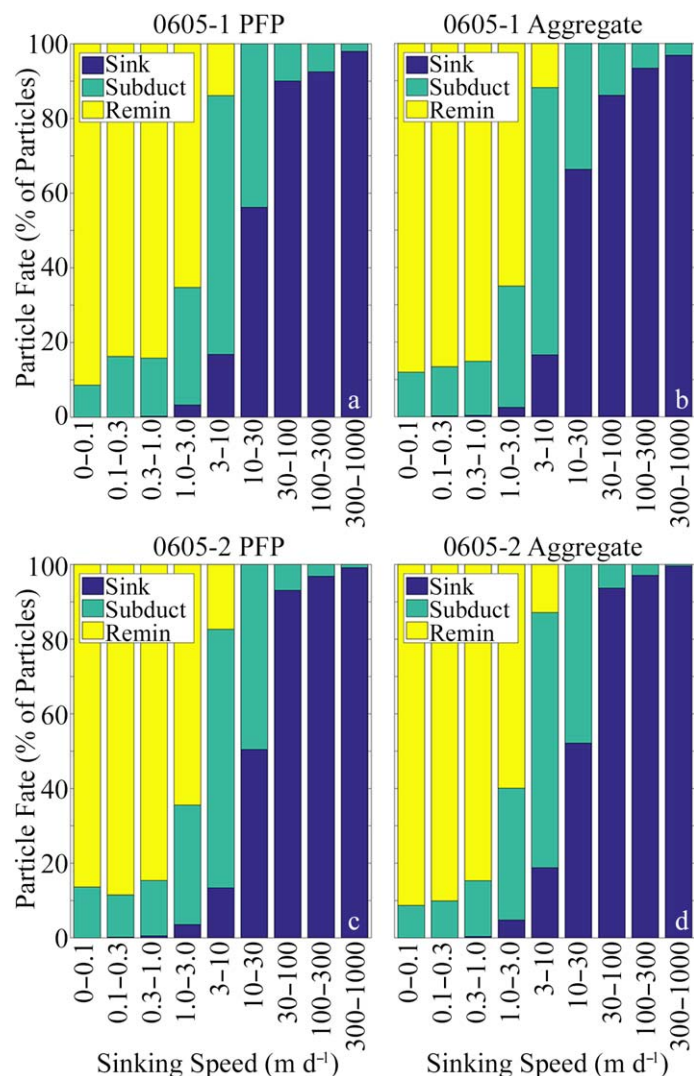
Fig. 6. Fate of particles as a function of sinking speed. Yellow is particles that did not cross the 100-m depth horizon during our 30-d simulation using the PFP parameterization (**a**) and (**c**) or the Agg parameterization (**b**) and (**d**). Teal is particles that were passively transported across the depth horizon. Blue is particles that gravitationally sank. (**a**) and (**b**) Cycle 0605-1. (**c**) and (**d**) Cycle 0605-2.

production rate) and λ (the remineralization rate) at the 95% confidence level (however, it was not significantly correlated with μ_1 and μ_2, the sinking speed parameters). Across the 13 cycles, passive POC flux ranged from 15 mg C m^{-2} d^{-1} (Cycle 0810-3) to 79 (Cycle 0704-1) mg C m^{-2} d^{-1} with a median and mean of 49 mg C m^{-2} d^{-1} and 46 mg C m^{-2} d^{-1}, respectively. Slightly reduced POC subduction estimates were found for the Agg parameterization (Fig. 5b), with subduction contributing between 7% (Cycle 0810-5) and 80% (Cycle 0704-2) of total POC export (median = 23%, mean = 26%). The contribution of passive flux was negatively correlated with α (the parameter most closely related to primary

productivity, $p < 0.01$) and was also negatively correlated with λ (though the relationship was not significant). For the Agg parameterization, passive flux ranged from 10 mg C m^{-2} d^{-1} (Cycle 0810-5) to 47 (Cycle 0704-2) mg C m^{-2} d^{-1}.

Particle fate (complete remineralization in the upper 100 m, subduction or gravitational export past the 100 m depth horizon) was predominantly determined by particle sinking speed (Fig. 6). Subducted particles primarily had sinking speeds in the range of 3–10 m d^{-1}, a result that was relatively constant for different cycles and particle sinking models (PFP or Agg parameterizations). Particles with slower sinking speeds were unlikely to cross the 100-m depth horizon during the 30-d model runs, while faster sinking particles were more likely to gravitationally sink than to be passively transported across the 100-m depth horizon. The consistent importance of intermediate speed sinking particles for subduction also explains passive transport differences between the Agg and PFP parameterizations, since the PFP parameterization predicted higher concentrations of particles with these sinking speeds than the Agg parameterization (Fig. 3).

In large part due to the differences in sinking speeds between gravitationally exported particles and passively exported particles (particles exported during the gravitational or advection subroutines, respectively), these two different mechanisms of export led to substantially different fates for exported particles. Gravitationally exported particles had a significantly deeper depth of remineralization than passively exported particles (Fig. 7). For the PFP parameterization, 40% of carbon that was gravitationally exported across the 100-m depth horizon was remineralized at a depth > 500 m (range = 7–69%). For the Agg parameterization, this figure was even higher (mean = 55%, range = 40–69%). By contrast, 57% of POC that was passively exported across the 100-m depth horizon was remineralized at a depth shallower than 150 m (range = 28–68%) for the PFP parameterization and 47% was remineralized shallower than 150 m for the Agg parameterization (range = 31–64%). This large difference suggests that particles that gravitationally sink from the surface ocean (and contribute to sediment trap and radionuclide disequilibrium-derived flux) are likely to have much longer carbon sequestration times than particles that were passively exported from the surface ocean. These particles also traveled substantially farther before being exported than the gravitationally exported particles. Across the two parameterizations, the median carbon-weighted distance traveled prior to export by particles that gravitationally sank across the 100-m depth horizon was 10 km, while the equivalent value for passively exported particles was 36 km.

The above analyses focused on the relative contribution of gravitational flux or subduction across the 100 m depth horizon. This depth was chosen because it is consistent with the depth of in situ sediment trap deployment and because CCE euphotic depths are seldom deeper than 100 m, but
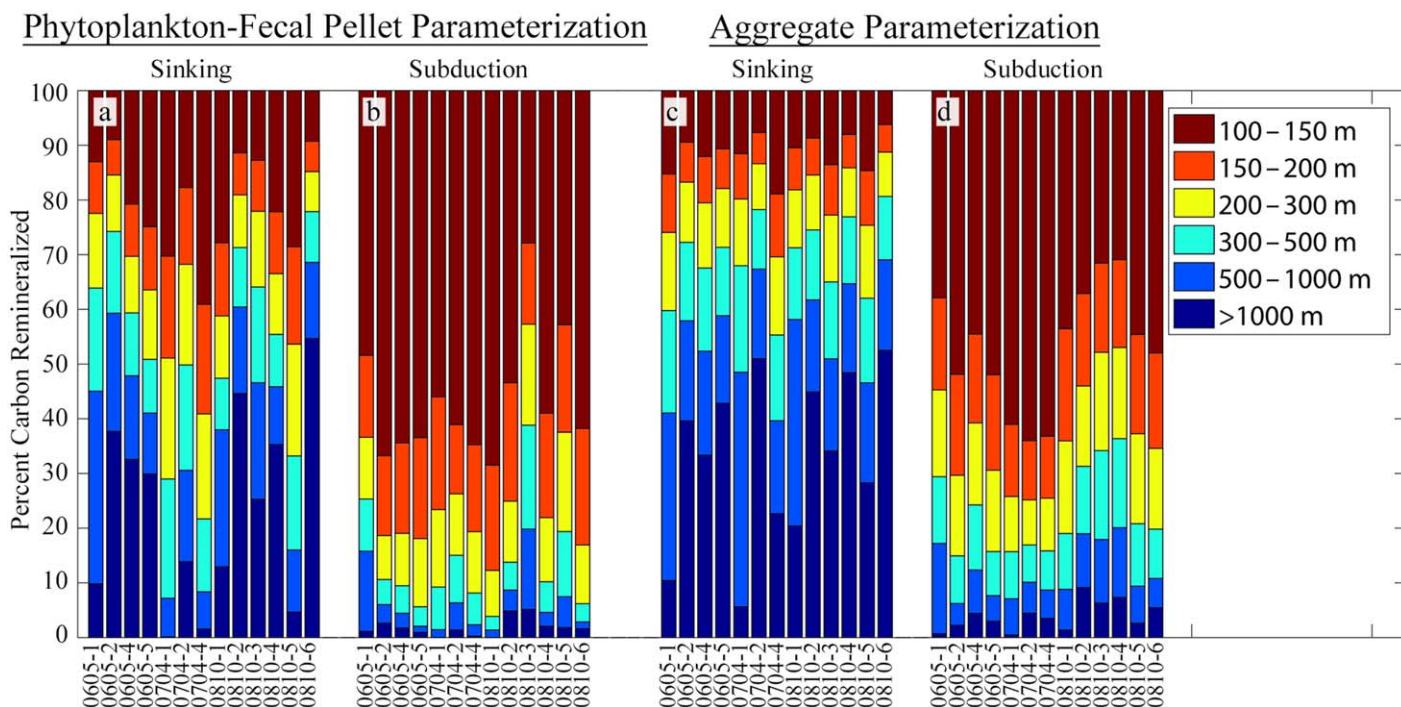
Phytoplankton-Fecal Pellet Parameterization
Aggregate Parameterization

Fig. 7. Depth horizons over which exported particulate carbon was remineralized in the three-dimensional model using the PFP parameterization (**a**, **b**) or the Agg parameterization (**c**, **d**). (**a**) and (**c**) particles that gravitationally sank across the 100-m depth horizon. (**b**) and (**d**) particles that were subducted across the 100-m depth horizon.

biological and chemical properties do not draw any distinction at this boundary. If instead we look at the relative contribution of subduction to POC export as a function of depth, we see that subduction becomes substantially more important for transport at shallower depth horizons (Fig. 8). At a depth of 25 m, subduction contributes over 50% of carbon flux for 11 of 13 cycles for both the PFP and Agg parameterizations. The median contribution of subduction to total flux across the two parameterizations was 73% at 25 m and decreased to 52% at 60 m. Continuing deeper, it was 27% at 100 m and 13% at 150 m. For comparison, the average seasonal mixed layer depth in the CCE typically varies from 20 m to 35 m, and the EZ on our cruises (as defined by the 1% light level) ranged from 24 m (0605-1) to 79 m (0605-2), but positive net primary production often extended down to the 0.1% light level, which ranged from 45 m to 116 m.

Uncertainty analysis

Broadly speaking, uncertainty in a modeling analysis such as ours can come from three distinct sources: (1) Uncertainty in the input parameters used in the model. (2) Uncertainty about the applicability of the chosen model. (3) Uncertainty about the generalizability of an individual study's specific context (location, time, currents, community, etc.). We attempted to address each of these potential uncertainty sources in turn.
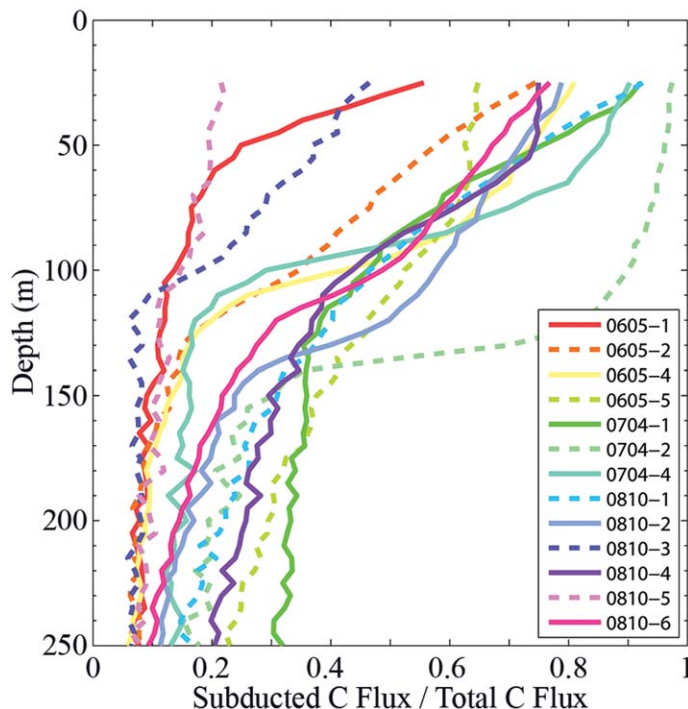

Fig. 8. Contributions of subduction to total POC flux as a function of depth for the PFP parameterization. Each line represents a different cycle.

To assess the impact of in situ measurement uncertainty on our results, we re-ran the three-dimensional model for each cycle (and for both the PFP and Agg parameterizations) after sequentially increasing or decreasing the in situ carbon export measurement by one standard deviation of the measurement uncertainty. Carbon export measurements were chosen for these analyses, both because they had the largest uncertainty and they were expected to have the greatest impact on model results. Unsurprisingly, modifying the export estimates used as inputs to the parameterizations had substantial impacts on both the parameterization of the models and on the amount of export predicted by the Lagrangian modeling approach. While the remineralization constant was relatively insensitive to changes in export, the parameters associated with mean sinking speed (μ_1 in the PFP parameterization; α and β in the Agg parameterization) changed substantially. The median value (across all cycles) of $\exp(\mu_1)$, (the median sinking speed of phytoplankton) increased from 0.5 m d^{-1} to 1.8 m d^{-1}, when export was increased from one standard error below the mean to one standard error above the mean. α and β showed more moderate changes (increasing from 42 to 48 and -1.2 to -1.1, respectively), but taken together these changes also had substantial impacts on mean sinking speeds and total gravitational flux. For the Agg parameterization, median gravitational flux increased from 73 mg C m^{-2} d^{-1} to 93 mg C m^{-2} d^{-1}, and for the PFP parameterization, it increased from 57 mg C m^{-2} d^{-1} to 71 mg C m^{-2} d^{-1} (although for individual cycles gravitational flux increased by up to a factor of 3). Although increasing the export input to the models had the expected effect of increasing gravitational flux in the Lagrangian models, it actually increased the vertical flux due to subduction by a slightly greater percentage (median subduction increased from 20.3 mg C m^{-2} d^{-1} to 31.9 mg C m^{-2} d^{-1} and 36.3 mg C m^{-2} d^{-1} to 61.6 mg C m^{-2} d^{-1} for the Agg and PFP parameterizations, respectively). The percentage of carbon export that resulted from subduction thus was relatively insensitive to changes in the input parameters (% subducted increased from 23.7% to 23.8% for the Agg parameterization and from 40.1% to 44.5% for the PFP parameterization, Table 4).

Uncertainty resulting from subjective choice of the shape of the particle sinking speed distribution was addressed through our use of two separate models with distinctly different distributions of sinking speed (Agg and PFP parameterizations, Fig. 3). The two parameterizations had important similarities and differences. Both parameterizations showed passive export to be an important, though not dominant portion of the total POC export (41% and 26% mean for PFP and Agg parameterizations, respectively) and found that sinking particles have a substantially greater remineralization length scale than subducted particles. They also agreed that subduction is a likely fate for particles sinking at intermediate speeds. However, the Agg parameterization suggested a

greater importance for gravitational sinking in total carbon sequestration, as it simultaneously had a deeper remineralization length scale for gravitational flux and a smaller contribution of passive flux to total export. Interestingly, the relative rank of different cycles with respect to percent contribution of passive flux to total export differed between the two parameterizations. Most obviously Cycle 0810-1 had the 9th (out of 13) highest passive contribution to export (46%) for the PFP parameterization and only the 3rd most for the Agg parameterization (15%).

We also addressed our assumption that remineralization was constant with depth for all particles, by developing an alternate model structure with temperature-dependence for λ. Particle remineralization is often mediated primarily by bacteria and other microorganisms, so we assumed that λ shows an exponential relationship to temperature of:

$$\lambda_{T=T_1} = \lambda_0 \times Q_{10}{}^{(T_1-T_0)/10} \tag{11}$$

where λ_0 is λ as solved previously from Eqs. 6–10, which we assume is representative of remineralization rates in the surface mixed layer. We used $Q_{10} = 2$ which is representative of typical bacterially-mediated marine processes (Kirchman et al. 1995; Kirchman et al. 2005). Using Eq. 11 and average temperature profiles for each cycle (surface temperatures varied from 12°C to 17°C and decreased to a temperature of ~ 4°C at 1000 m depth), remineralization rates decreased by up to 60% at 1000 m depth. This led to a predictable, though relatively minor, increase in carbon export out of the upper 100 m and in the overall depth of remineralization for organic matter exported by sinking or subduction (Supporting Information Figs. 4, 5). However, it did not substantially change the relative contributions of sinking and subduction to export.

Passive flux varied substantially between cycles. The coefficient of variation (standard deviation/mean) was 39% for the PFP parameterization and 43% for the Agg parameterization, while the spread was 15–79 mg C m^{-2} d^{-1} and 10–47 mg C m^{-2} d^{-1} for the two parameterizations. These differences likely reflect true variability in the system. Our study region has several biogeochemically-distinct regions (the Southern California Bight, an upwelling center near Point Conception, a transition region near the spatially-variable California Current core, and an offshore oligotrophic environment), each with its own distinct floral and faunal community that varies in time (Venrick 1998; Lavaniegos and Ohman 2007). Across the domain, different sectors can be dominated by picoplankton ($> 80\%$ of Chl *a* in the < 3-μm size fraction) or microplankton ($> 80\%$ of Chl *a* in the > 20-μm size fraction, Goericke 2011). It is thus not surprising to find substantial variability in export patterns. Our finding that passive flux is a more important contributor to total flux in the oligotrophic regions with small phytoplankton and zooplankton taxa (and hence lower mean

sinking speeds) was a robust result that held for both parameterizations.

Discussion

Passive export of particles

All particles in our models are simultaneously sinking and being advected vertically and horizontally. Thus, the dichotomy that we use to separate them into particles that were subducted or gravitationally sank (based on which process transported them across the 100-m depth horizon) may seem arbitrary. However, when summed over thousands of particles, our approach determines the proportion of vertical motion driven by sinking or advection. In essence, this can be considered a probabilistic view of particle transport. The relative magnitudes of the sinking and vertical advection velocity vectors determine the likelihood that a particle will be counted as sinking or subducted. Crucially, this relative contribution of sinking or advection also affects typical in situ measurements of carbon flux. Assuming negligible hydrodynamic biases, particle accumulation within sediment traps is determined only by particle sinking speeds. Subduction events will not increase the amount of particles collected by the sediment trap, because as the streamlines diverge around the trap tube the dominant viscous forces (Reynolds numbers typically < 0.1) will ensure that the particles are transported around the trap, rather than into it. The possibility of turbulent motion near the trap interface could potentially introduce subducted particles, however the use of a salt brine and design of the baffle on the top of the tube minimizes mixing (Knauer et al. 1979). Indeed, our own measurements of the salinity of the brine before and after deployment and recovery showed no dilution of the preserved brine with ambient seawater (Krause et al. 2015). It is thus likely that advection is a negligible source of particle flux into our sediment traps. Similarly, a neutrally buoyant sediment trap will be transported with the subduction event and will not collect the advected particles. Radionuclide disequilibrium methods (^{238}U : ^{234}Th and ^{210}Pb : ^{210}Po) will also fail to register a signal from subduction, since advection will transport the parent and daughter isotopes together. This is not to say that subducted particles cannot be collected by deeper sediment traps. Indeed, particles that are advected past the 100-m depth horizon in our models may cross the 150-m depth horizon by gravitational flux. Nevertheless, the subduction portion of the flux must be considered as an extra carbon transport term that is in addition to the flux measured by sediment traps or radionuclide disequilibrium methods.

The high export rates due to subduction suggested by our models (10–79 mg C m^{-2} d^{-1}; 7–90% of total export) have additional implications for particle transport in the ocean interior. It is commonly assumed that large aggregates collected by in situ pumps are representative of sinking particles

(Bishop et al. 2012; Mcdonnell et al. 2015*b*). However, our results suggest that many particles found in the deep epipelagic and shallow mesopelagic may have been transported there by subduction. Since subducted particles have substantially lower mean sinking speeds than gravitationally exported particles, they also have greater residence times in the deep epipelagic and thus contribute disproportionately to particulate standing stock (sampled by pumps) relative to their contribution to vertical flux. The importance of passive export may also explain a discrepancy between the prevalence of small phytoplankton biomarkers in deep-water samples (Lomas and Moran 2011; Sohrin et al. 2011), despite their relatively small contribution to gravitational flux (Rodier and Le Borgne 1997; Waite et al. 2000; Stukel and Landry 2010). Picoplankton may get incorporated into aggregates with relatively low mineral content and hence fairly slow sinking speeds. These aggregates would then be more likely to be subducted from the surface ocean and hence would not be captured by sediment traps, though they would contribute substantially to the shallow mesopelagic standing stock.

As mentioned above, our models suggest an important role for particles with intermediate sinking speeds (e.g., 1–10 m d^{-1}) in passive transport of carbon to depth. Because particle remineralization in the surface ocean is typically quite high, most slowly-sinking organic particles (< 1 m d^{-1}) are almost entirely remineralized within the EZ. Meanwhile, particles with sinking speeds ≥ 30 m d^{-1} will be transported across any given depth horizon primarily by gravitational sinking rather than advection. The intermediate sinking rate particles that likely contribute disproportionately to passive export are often absent from biogeochemical models. For instance, the NEMURO model has a single sinking-particle compartment with a sinking speed of 40 m d^{-1} (Kishi et al. 2007). To compare how our results with continuous sinking speed spectra might differ from typical biogeochemical models that have only a single sinking speed for detritus, we developed a simple single-sinking speed parameterization such that Eq. 3 can be rewritten as: $PP_{SS}(0) = {}^{14}CPP \times (1-\varepsilon)$ and $PP_{SS}(\omega) = {}^{14}CPP \times \varepsilon$, where ε is the fraction of particles that are sinking and ω is the sinking speed of the sinking particles. We chose 100 m d^{-1} as a representative speed for sinking particles in the ocean (Mcdonnell and Buesseler 2010), and solved Eqs. 6, 7, 10 as before then ran the new particle model in the three-dimensional framework. Compared to either the Agg or PFP parameterizations, the Single Speed parameterization had a substantially lower fraction of carbon transported to depth by passive export (median = 14%, compared to 44% and 23% for the PFP and Agg parameterizations, respectively). This shows that biogeochemical models that assign only a single sinking speed to detritus may give biased results if used to assess the relative fraction of particle export mediated by subduction.

The relative importance of subduction is also dependent on the choice of depth horizon. Conceptually, the ideal choice of depth horizon might be either the depth of the EZ or the seasonal thermocline, but each of these has distinct spatiotemporal variability that was not fully quantified throughout our broader study region. Instead, we chose 100 m for this study because it was a consistent depth used for the in situ measurements of gravitational flux (sediment traps and ^{234}Th) that we incorporated when parameterizing the models and also because it is a depth that typically incorporates the entirety of the EZ and mixed layer throughout the CCE. If deeper depth horizons were chosen, the contribution of subduction to total export would decrease, since (as noted previously) the remineralization length scale is longer for gravitationally sinking particles than for subducted particles. If we consider increasingly deeper depth horizons the proportion of total particulate export resulting from subduction in the PFP parameterization decreases from 44% (median across all cycles at 100 m) to 29%, 22%, 16%, and 11% for depths of 125 m, 150 m, 200 m, and 250 m, respectively. For the Agg parameterization, the corresponding percent subducted decreases from 23% at 100 m to 14%, 11%, 10%, and 8%. Conversely (as explored below), a shallower depth horizon would indicate a greater importance for subduction.

Particle dynamics and carbon export

By using gravitational export, POC standing stock, and particle formation (^{14}CPP) to parameterize our models, we are implicitly determining mean particle turnover times (and remineralization rate, λ) that relate to the length of time between when POC is created and when it is finally remineralized to CO_2. This is distinctly different, however, from the length of time that a particle spends in any given form (e.g., as a living phytoplankter, a copepod fecal pellet, or a 1-mm phytodetrital aggregate). For instance, a phytoplankter may be repackaged into an aggregate, or portions of its carbon may be converted into zooplankton and/or fecal pellets before it is inevitably remineralized somewhere in the water column. Our modeling approach omits the complex particle transformation dynamics inherent in many models of particle size spectra (Jackson 2001; Stemmann et al. 2004; Burd and Jackson 2009) in favor of a simpler scheme that can be directly parameterized using in situ observations. Thus while our approach is well suited for its intended purpose of assimilating in situ measurements to allow diagnostic modeling of short-term particle transport during a field campaign, it is not appropriate for predictive modeling of particle transport. For such applications, it will become necessary to understand how pelagic ecology and biogeochemistry interact to shape the particle sinking speed spectrum.

The in situ biogeochemical measurements incorporated into this study clearly show distinct differences in mean particle sinking speeds. For the PFP parameterization, the mean sinking speed of particles created in the EZ ranged from 2.5 m d^{-1} to 46 m d^{-1}, while for the Agg parameterization it varied from 7.8 m d^{-1} to 73 m d^{-1}. These differences drive substantial variability in the fate of sinking particles; hence, it is important to understand the mechanisms driving changes in sinking speed. At its most basic level, particle sinking speeds are determined by size, shape, porosity, and excess density. However, these properties are difficult to measure on naturally occurring particles and marine snow and are constantly changing as particles evolve due to chemical, physical, and ecological processes. For instance, density likely increases for many sinking particles when bacteria preferentially remineralize organic matter relative to $CaCO_3$, Si, or lithogenic minerals (Armstrong et al. 2002). Processes of differential settling, coagulation, disaggregation, and deflation constantly re-work marine snow, changing the porosity, size, and shape of these aggregates as they sink (Burd and Jackson 2009; Lombard and Kiorboe 2010). Mesozooplankton feeding at all depths in the ocean also continually re-shape the particle size spectrum by efficiently packaging smaller particles into larger fecal pellets (Wilson et al. 2008; Turner 2015) or by fragmenting aggregates through swimming-induced turbulence or partial consumption of detritus (Lampitt et al. 1990; Dilling and Alldredge 2000). The complexity of these processes highlight our need for direct in situ measurements of particle size, shape, and sinking speeds across a variety of ecosystem states to progress toward a predictive framework for particle sinking speeds in the ocean.

Sinking speed alone does not control particle fate; remineralization rates play an equally important role in determining the depth of organic matter penetration into the ocean. For instance, 35% and 15% of the variability in the relative contribution of passive flux to total flux could be explained by a linear relationship with remineralization constant (λ), for the PFP and Agg parameterizations, respectively. Water parcels with low remineralization rates relied on a relatively greater role for subduction in vertical carbon transport. However, by assigning a single remineralization constant to all particles for a given water parcel, our modeling approach oversimplifies the multiplicity of processes that can degrade organic matter in the ocean. Remineralization rates are likely to be quite different for fecal pellets composed of undigested material, aggregates formed from mucous feeding structures, or fresh phytodetritus. Particle remineralization rates in the ocean likely vary widely and hence might be more accurately described by probability distributions in a similar way to how we depicted the sinking speed distributions. Ascertaining how sinking speed and remineralization rate might covary is a non-trivial task. For instance, should we anticipate that phytodetritus in surface layers (small and readily available to protistan grazers) is both slowly sinking and more rapidly remineralized and that large rapidly sinking fecal pellets have low remineralization rates because mesozooplankton have already utilized the most labile fractions of the organic matter (hence a negative
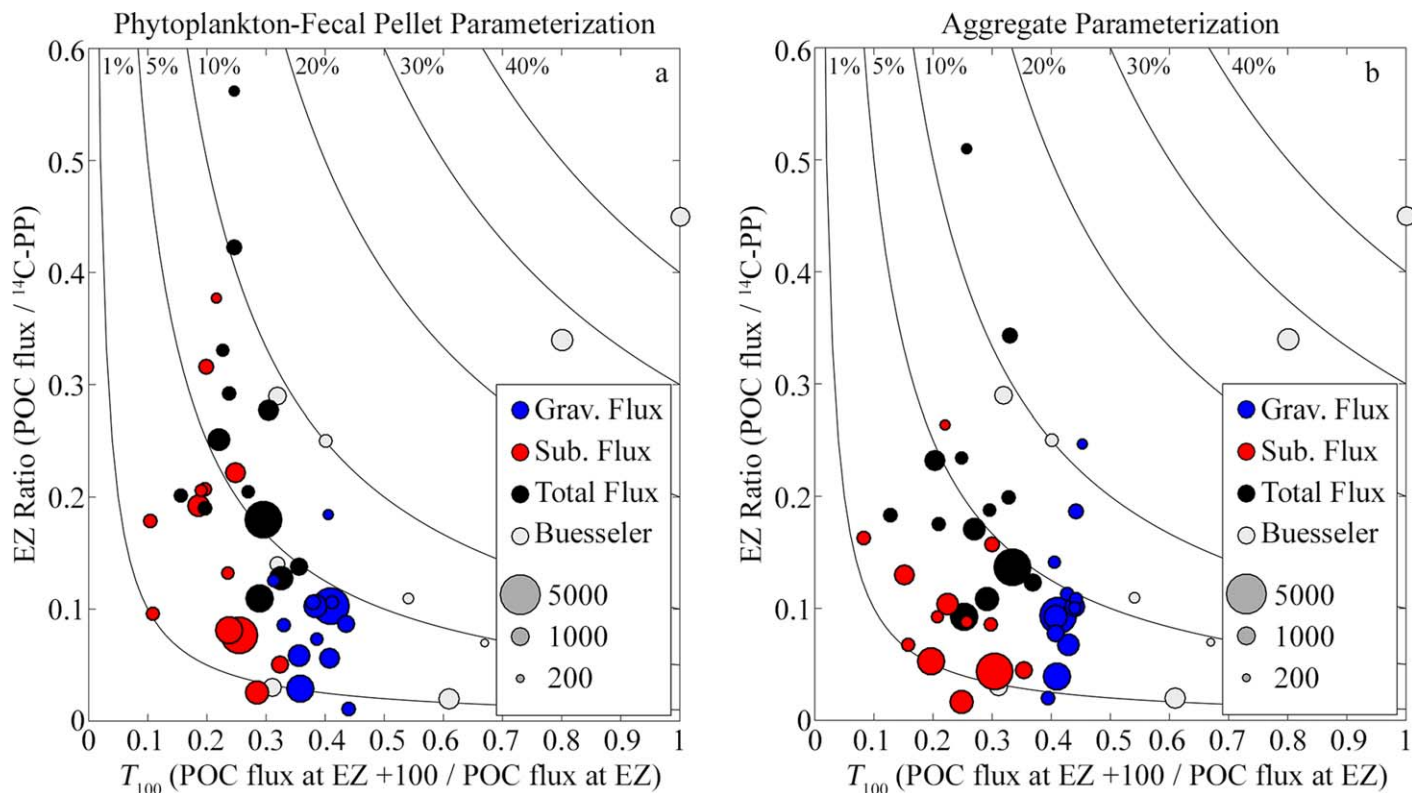
Fig. 9. Plot of EZ ratio (POC flux at the base of the EZ/^{14}CPP) vs. T_{100} (POC flux at 100 m below EZ/POC flux at EZ) for PFP parameterization (**a**) and Agg parameterization (**b**). Size of circle is proportional to primary productivity (mg C m^{-2} d^{-1}). Blue symbols are gravitational flux. Red symbols are for subduction. Black symbols are for total POC flux. Light gray is summary data from other regions reported in Buesseler and Boyd (2009). Black contours show percent of ^{14}CPP exported past EZ + 100.

relationship between sinking speed and remineralization rate)? Or should we assume that rapidly sinking aggregates are sites of extensive bacterial colonization and remineralization (positive relationship)? Are remineralization rates controlled by the concentration of grazers (Gonzalez and Smetacek 1994; Jackson and Checkley 2011), bacteria (Azam 1998; Steinberg et al. 2008), or temperature (Laws et al. 2000)? New technologies are beginning to allow us to probe these questions (McDonnell et al. 2015a), but our current understanding is still limited. Hence, we took the Occam's razor approach of determining a single remineralization rate for particles produced during a particular cycle, regardless of sinking speed. We believe, however, that by using remineralization rates that were determined independently for each cycle from the in situ measurements, our modeling approach makes an important advance over most models that assume a single a priori remineralization rate (or a single temperature-dependent remineralization function) for all particles everywhere in the ocean.

The fate of gravitationally sinking and subducted particles

The primary motivation for most studies of vertical carbon transport in the ocean is a desire to understand either

the ocean's ability to sequester carbon or the sources of energy for organisms in the mesopelagic and benthos. For both of these questions, quantifying total export (which should balance new production, sensu Eppley and Peterson 1979) is not sufficient because the remineralization length scale determines how far into the ocean exported organic matter penetrates, and hence whether it is remineralized in the upper mesopelagic, feeds benthic organisms, or is sequestered for long periods of time in the abyssal ocean. Thus, understanding controls on flux attenuation can be crucial to determining the biogeochemical and ecological fate of export production.

Following Buesseler and Boyd (2009), we can simultaneously consider export at the base of the EZ and flux attenuation by comparing the EZ-ratio (the ratio of export at the base of the EZ to ^{14}CPP) to the T_{100} ratio (POC flux 100 m below the EZ to POC flux at the base of the EZ). While Buesseler and Boyd (2009) considered only gravitational flux, we extend their analysis to include subductive flux and total flux (subduction + gravitational, Fig. 9). Comparing our results to other regions, it is clear that the CCE has moderate to low export sequestration efficiency, with typically 5–10% of ^{14}CPP transported to a depth 100 m deeper than the EZ. Relatively inefficient gravitational carbon sequestration

resulted primarily from a low EZ-ratio (with a moderate T_{100} for gravitational flux). In contrast to gravitational flux, POC transport resulting from subduction had a relatively high EZ-ratio, suggesting that (in contrast to our previous results which were normalized to a constant 100 m depth horizon) rates of POC subduction out of the EZ were typically greater than rates of gravitational flux. However, subducted material also had a consistently lower T_{100}, implying that most of this material was rapidly remineralized in the deep epipelagic zone and hence has low sequestration potential. This highlights an important dichotomy in the way subducted and sinking POC should be considered: while subduction may play an important role in the total EZ carbon and nitrogen balances, a focus on gravitational flux is justified based on its higher potential for deep ocean carbon sequestration.

So far, we have discussed only POC export, but passive transport of DOM has been hypothesized to also play an important role in the marine carbon budget (Copin-Montégut and Avril 1993; Carlson et al. 1994; Hansell et al. 2009). DOM is produced in surface waters by phytoplankton exudation, sloppy feeding by grazers, particle solubilization, and other processes (Carlson 2002). The labile fraction of this material is then rapidly degraded by surface microbes, leading to gradual conversion of this fresh DOM to a more refractory state (Hansell et al. 2012). On CCE LTER survey cruises, $H^{14}CO_3^-$ uptake experiments showed that DOC production rates were approximately 20% of particulate ^{14}CPP. If we consider DOM to be identical to POC, but with no sinking rate, Fig. 6 would suggest that DOM would be a minor component of export out of the EZ and a negligible component of sequestration in deeper waters. However, since DOM has substantially different removal processes (primarily utilization by free-living bacteria) than POC (primarily grazing and degradation by attached microbes), it likely also has different remineralization rates. Thus, determining the potential increased organic matter transport mediated by subduction (or vertical mixing) of DOM will require a different analysis.

Conclusions

In this study, we set out to address the potential contributions of sinking particles and subducted particles to carbon export, and to ascertain how the biogeochemical fate of POC differs for these different pathways of export. To accomplish these goals, we developed a novel approach for assimilating in situ primary production, POC standing stock, and gravitational export measurements into a Lagrangian particle tracking model. Our study clearly demonstrates the importance of subduction for the carbon and nitrogen balance in the EZ of the CCE. However, there remained a substantial (approximately factor of 2) difference between estimates of passive export using different particle sinking spectrum shapes designed to capture the dynamics predicted by two different

conceptual models of particle sinking in the ocean (export driven by packaging of phytoplankton into fecal pellets or by aggregates). Furthermore, in situ conditions clearly play a very large role in the relative importance of subduction (at 100 m, percent subducted varied from 14% to 90% for the PFP parameterization). Thus, understanding spatiotemporal variability in passive transport—and the extent to which it will be altered by climate change—clearly requires a predictive understanding of individual particle sinking speeds and remineralization rates. Future advances will require careful field work to constrain in situ particle distributions (Checkley et al. 2008; Picheral et al. 2010), sinking speeds (Trull et al. 2008; Lee et al. 2009; McDonnell and Buesseler 2010; Jackson et al. 2015), and remineralization rates (McDonnell et al. 2015a) in the epi- and mesopelagic. Crucially, these studies must also quantify particle transformation mechanisms (primary production, aggregation and disaggregation, grazing and fecal pellet production, bacterial remineralization) that respond to depth-specific food web dynamics. With such information, it should be possible to construct dynamic particle models that are parameterized using in situ measurements, but allow for spatiotemporal variability in particle sinking speed spectra driven by local physical, chemical, and ecological conditions.

Data availability statement

Data used in this study are available on the CCE LTER Datazoo website.

References

Alldredge, A. 1998. The carbon, nitrogen and mass content of marine snow as a function of aggregate size. Deep-Sea Res. Part I Oceanogr. Res. Pap. **45**: 529–541. doi:10.1016/S0967-0637(97)00048-4

Alldredge, A. L., and C. Gotschalk. 1988. In situ settling behavior of marine snow. Limnol. Oceanogr. **33**: 339–351. doi:10.419/lo.1988.33.3.0339

Armstrong, R. A., C. Lee, J. I. Hedges, S. Honjo, and S. G. Wakeham. 2002. A new, mechanistic model for organic carbon fluxes in the ocean based on the quantitative association of POC with ballast minerals. Deep-Sea Res. Part II Top. Stud. Oceanogr. **49**: 219–236. doi:10.1016/S0967-0645(01)00101-1

Azam, F. 1998. Microbial control of oceanic carbon flux: The plot thickens. Science **280**: 694–696. doi:10.1126/science.280.5364.694

Bacon, M. P., J. K. Cochran, D. Hirschberg, T. R. Hammar, and A. P. Fleer. 1996. Export flux of carbon at the equator during the EqPac time-series cruises estimated from Th-234 measurements. Deep-Sea Res. Part II Top. Stud. Oceanogr. **43**: 1133–1153. doi:10.1016/0967-0645(96)00016-1

Bienfang, P. K. 1980. Herbivore diet affects fecal pellet settling. Can. J. Fish. Aquat. Sci. **37**: 1352–1357. doi:10.1139/f80-173

Bishop, J. K. B., P. J. Lam, and T. J. Wood. 2012. Getting good particles: Accurate sampling of particles by large volume in-situ filtration. Limnol. Oceanogr.: Methods **10**: 681–710. doi:10.419/lom.2012.10.681

Boyd, P. W., and T. W. Trull. 2007. Understanding the export of biogenic particles in oceanic waters: Is there consensus? Prog. Oceanogr. **72**: 276–312. doi:10.1016/j.pocean.2006.10.007

Broquet, G., C. A. Edwards, A. M. Moore, B. S. Powell, M. Veneziani, and J. D. Doyle. 2009. Application of 4D-variational data assimilation to the California Current System. Dyn. Atmos. Oceans **48**: 69–92. doi:10.1016/j.dynatmoce.2009.03.001

Buesseler, K. O., and others. 2007. Revisiting carbon flux through the ocean's twilight zone. Science **316**: 567–570. doi:10.1126/science.1137959

Buesseler, K. O., and P. W. Boyd. 2009. Shedding light on processes that control particle export and flux attenuation in the twilight zone of the open ocean. Limnol. Oceanogr. **54**: 1210–1232. doi:10.419/lo.2009.54.4.1210

Burd, A. B., and G. A. Jackson. 2009. Particle aggregation. Ann. Rev. Mar. Sci. **1**: 65–90. doi:10.1146/annurev.marine.010908.163904

Burd, A. B., and others. 2010. Assessing the apparent imbalance between geochemical and biochemical indicators of meso- and bathypelagic biological activity: What the @$#! is wrong with present calculations of carbon budgets? Deep-Sea Res. Part II Top. Stud. Oceanogr. **57**: 1557–1571. doi:10.1016/j.dsr2.2010.02.022

Carlson, C. A. 2002. Production and removal processes. In D. A. Hansell and C. A. Carlson [eds.], Biogeochemistry of marine dissolved organic matter. Academic Press. 91–151.

Carlson, C. A., H. W. Ducklow, and A. F. Michaels. 1994. Annual flux of dissolved organic carbon from the euphotic zone in the northwestern Sargasso Sea. Nature **371**: 405–408. doi:10.138/371405a0

Carlson, C. A., and H. W. Ducklow. 1995. Dissolved organic carbon in the upper ocean of the central Equatorial Pacific Ocean, 1992: Daily and finescale vertical variations. Deep-Sea Res. Part II Top. Stud. Oceanogr. **42**: 639–656. doi:10.1016/0967-0645(95)00023-J

Chai, F., R. C. Dugdale, T. H. Peng, F. P. Wilkerson, and R. T. Barber. 2002. One-dimensional ecosystem model of the equatorial Pacific upwelling system. Part I: Model development and silicon and nitrogen cycle. Deep-Sea Res. Part II Top. Stud. Oceanogr. **49**: 2713–2745. doi:10.116/S0967-0645(02)00055-3

Checkley, D. M., R. E. Davis, A. W. Herman, G. A. Jackson, B. Beanlands, and L. A. Regier. 2008. Assessing plankton and other particles *in situ* with the SOLOPC. Limnol. Oceanogr. **43**: 2123–2136. doi:10.4319/lo.2008.53.5_part_2.2123

Conover, R. J. 1966. Assimilation of organic matter by zooplankton. Limnol. Oceanogr. **11**: 338–345. doi:10.4319/lo.1966.11.3.0338

Copin-Montégut, G., and B. Avril. 1993. Vertical distribution and temporal variation of dissolved organic carbon in the North-Western Mediterranean Sea. Deep-Sea Res. Part I Oceanogr. Res. Pap. **40**: 1963–1972. doi:10.1016/0967-0637(93)90041-Z

De La Rocha, C. L., and U. Passow. 2007. Factors influencing the sinking of POC and the efficiency of the biological carbon pump. Deep-Sea Res. Part II Top. Stud. Oceanogr. **54**: 639–658. doi:10.1016/j.dsr2.2007.01.004

Dilling, L., and A. L. Alldredge. 2000. Fragmentation of marine snow by swimming macrozooplankton: A new process impacting carbon cycling in the sea. Deep-Sea Res. Part I Oceanogr. Res. Pap. **47**: 1227–1245. doi:10.1016/S0967-0637(99)00105-3

Doyle, J. D., Q. F. Jiang, Y. Chao, and J. Farrara. 2009. High-resolution real-time modeling of the marine atmospheric boundary layer in support of the AOSN-II field campaign. Deep-Sea Res. Part II Top. Stud. Oceanogr. **56**: 87–99. doi:10.1016/j.dsr2.2008.08.009

Ducklow, H. W., D. K. Steinberg, and K. O. Buesseler. 2001. Upper ocean carbon export and the biological pump. Oceanography **14**: 50–58. doi:10.5670/oceanog.2001.06

Dunne, J. P., R. A. Armstrong, A. Gnanadesikan, and J. L. Sarmiento. 2005. Empirical and mechanistic models for the particle export ratio. Global Biogeochem. Cycles **19**: GB4026. doi:10.1029/2004GB002390

Eppley, R. W., and B. J. Peterson. 1979. Particulate organic matter flux and planktonic new production in the deep ocean. Nature **282**: 677–680. doi:10.1038/282677a0

Estapa, M. L., D. A. Siegel, K. O. Buesseler, R. H. R. Stanley, M. W. Lomas, and N. B. Nelson. 2015. Decoupling of net community and export production on submesoscales. Global Biogeochem. Cycles **29**: 1266–1282. doi:10.1002/2014GB004913

Fasham, M. J. R., H. W. Ducklow, and S. M. Mckelvie. 1990. A nitrogen-based model of plankton dynamics in the oceanic mixed layer. J. Mar. Res. **48**: 591–639. doi:10.1357/002224090784984678

Franks, P. J. S. 2009. Planktonic ecosystem models: Perplexing parameterizations and a failure to fail. J. Plankton Res. **31**: 1299–1306. doi:10.1093/plankt/fbp069

Goericke, R. 2011. The size structure of marine phytoplankton - what are the rules? Cal. Coop. Ocean. Fish. Invest. Rep. **52**: 198–204.

Goes, J. I., T. Saino, H. Oaku, J. Ishizaka, C. S. Wong, and Y. Nojiri. 2000. Basin scale estimates of sea surface nitrate and new production from remotely sensed sea surface temperature and chlorophyll. Geophys. Res. Lett. **27**: 1263–1266. doi:10.1029/1999GL002353

Gonzalez, H. E., and V. Smetacek. 1994. The possible role of the cyclopoid copepod *Oithona* in retarding vertical flux

of zooplankton fecal material. Mar. Ecol. Prog. Ser. **113**: 233–246. doi:10.3354/meps113233

Gruber, N., Z. Lachkar, H. Frenzel, P. Marchesiello, M. Münnich, J. C. McWilliams, T. Nagai, and G. K. Plattner. 2011. Eddy-induced reduction of biological production in eastern boundary upwelling systems. Nat. Geosci. **4**: 787–792. doi:10.1038/ngeo1273

Guidi, L., G. A. Jackson, L. Stemmann, J. C. Miquel, M. Picheral, and G. Gorsky. 2008. Relationship between particle size distribution and flux in the mesopelagic zone. Deep-Sea Res. Part I Oceanogr. Res. Pap. **55**: 1364–1374. doi:10.1016/j.dsr.2008.05.014

Hansell, D. A., C. A. Carlson, D. J. Repeta, and R. Schlitzer. 2009. Dissolved organic matter in the ocean: A controversy stimulates new insights. Oceanography **22**: 202–211. doi:10.5670/oceanog.2009.109

Hansell, D. A., C. A. Carlson, and R. Schlitzer. 2012. Net removal of major marine dissolved organic carbon fractions in the subsurface ocean. Global Biogeochem. Cycles **26**: 1–9. doi:10.1029/2011GB004069

Henson, S. A., R. Sanders, E. Madsen, P. J. Morris, F. Le Moigne, and G. D. Quartly. 2011. A reduced estimate of the strength of the ocean's biological carbon pump. Geophys. Res. Lett. **38**. doi:10.1029/2011GL046735

Hodur, R. M., and J. D. Doyle. 1999. The coupled ocean/atmosphere mesoscale prediction system (COAMPS). Coast. Ocean Predict. **56**: 125–155. doi:10.1029/CE056p0125

Honjo, S., S. J. Manganini, R. A. Krishfield, and R. Francois. 2008. Particulate organic carbon fluxes to the ocean interior and factors controlling the biological pump: A synthesis of global sediment trap programs since 1983. Prog. Oceanogr. **76**: 217–285. doi:10.1016/j.pocean.2007.11.003

Jackson, G. A. 2001. Effect of coagulation on a model planktonic food web. Deep-Sea Res. Part I Oceanogr. Res. Pap. **48**: 95–123. doi:10.1016/S0967-0637(00)00040-6

Jackson, G. A., R. Maffione, D. K. Costello, A. L. Alldredge, B. E. Logan, and H. G. Dam. 1997. Particle size spectra between 1 μm and 1 cm at Monterey Bay determined using multiple instruments. Deep-Sea Res. Part I Oceanogr. Res. Pap. **44**: 1739–1767. doi:10.1016/S0967-0637(97)00029-0

Jackson, G. A., and D. M. Checkley. 2011. Particle size distributions in the upper 100 m water column and their implications for animal feeding in the plankton. Deep-Sea Res. Part I Oceanogr. Res. Pap. **58**: 283–297. doi:10.1016/j.dsr.2010.12.008

Jackson, G. A., D. M. Checkley, Jr., and M. Dagg. 2015. Settling of particles in the upper 100 m of the ocean detected with autonomous profiling floats off California. Deep-Sea Res. Part I Oceanogr. Res. Pap. **99**: 75–86. doi:10.1016/j.dsr.2015.02.001

Kahler, P., A. Oschlies, H. Dietze, and W. Koeve. 2010. Oxygen, carbon, and nutrients in the oligotrophic eastern subtropical North Atlantic. Biogeosciences **7**: 1143–1156. doi:10.5194/bg-7-1143-2010

Karleskind, P., M. Levy, and L. Memery. 2011. Subduction of carbon, nitrogen, and oxygen in the northeast Atlantic. J. Geophys. Res. Oceans **116**: 1–17. doi:10.1029/2010JC006446

Kirchman, D. L., J. H. Rich, and R. T. Barber. 1995. Biomass and biomass production of heterotrophic bacteria along 140°W in the equatorial Pacific - effect of temperature on the microbial loop. Deep-Sea Res. Part II Top. Stud. Oceanogr. **42**: 603–619. doi:10.1016/0967-0645(95)00021-H

Kirchman, D. L., R. R. Malmstrom, and M. T. Cottrell. 2005. Control of bacterial growth by temperature and organic matter in the Western Arctic. Deep-Sea Res. Part II Top. Stud. Oceanogr. **52**: 3386–3395. doi:10.1016/j.dsr2.2005.09.005

Kishi, M. J., and others. 2007. NEMURO - a lower trophic level model for the North Pacific marine ecosystem. Ecol. Modell. **202**: 12–25. doi: 10.1016/j.ecolmodel.2006.08.021

Knauer, G. A., J. H. Martin, and K. W. Bruland. 1979. Fluxes of particulate carbon, nitrogen, and phosphorus in the upper water column of the Northeast Pacific. Deep Sea Res. Part A Oceanogr. Res. Pap. **26**: 97–108. doi:10.1016/0198-0149(79)90089-X

Krause, J. W., M. A. Brzezinski, R. Goericke, M. R. Landry, M. D. Ohman, M. R. Stukel, and A. G. Taylor. 2015. Variability in diatom contributions to biomass, organic matter production and export across a frontal gradient in the California Current Ecosystem. J. Geophys. Res. Oceans **120**: 1032–1047. doi:10.1002/2014JC010472

Lampitt, R. S., T. Noji, and B. Von Bodungen. 1990. What happens to zooplankton fecal pellets? Implications for material flux. Mar. Biol. **104**: 15–23. doi:10.1007/BF01313152

Landry, M. R., M. D. Ohman, R. Goericke, M. R. Stukel, and K. Tsyrklevich. 2009. Lagrangian studies of phytoplankton growth and grazing relationships in a coastal upwelling ecosystem off Southern California. Prog. Oceanogr. **83**: 208–216. doi:10.1016/j.pocean.2009.07.026

Landry, M. R., M. D. Ohman, R. Goericke, M. R. Stukel, K. A. Barbeau, R. Bundy, and M. Kahru. 2012. Pelagic community responses to a deep-water front in the California Current Ecosystem: Overview of the A-Front Study. J. Plankton Res. **34**: 739–748. doi:10.1093/plankt/fbs025

Lavaniegos, B. E., and M. D. Ohman. 2007. Coherence of long-term variations of zooplankton in two sectors of the California Current System. Prog. Oceanogr. **75**: 42–69. doi:10.1016/j.pocean.2007.07.002

Law, C. S., A. J. Watson, M. I. Liddicoat, and T. Stanton. 1998. Sulphur hexafluoride as a tracer of biogeochemical and physical processes in an open-ocean iron fertilisation experiment. Deep-Sea Res. Part II Top. Stud. Oceanogr. **45**: 977–994. doi:10.1016/S0967-0645(98)00022-8

Laws, E. A., P. G. Falkowski, W. O. Smith, H. Ducklow, and J. J. Mccarthy. 2000. Temperature effects on export

production in the open ocean. Global Biogeochem. Cycles **14**: 1231–1246. doi:10.1029/1999GB001229

Laws, E. A., E. D'sa, and P. Naik. 2011. Simple equations to estimate ratios of new or export production to total production from satellite-derived estimates of sea surface temperature and primary production. Limnol. Oceanogr.: Methods **9**: 593–601. doi:10.4319/lom.2011.9.593

Lee, C., and others. 2009. Particulate organic matter and ballast fluxes measured using time-series and settling velocity sediment traps in the northwestern Mediterranean Sea. Deep-Sea Res. Part II Top. Stud. Oceanogr. **56**: 1420–1436. doi:10.1016/j.dsr2.2008.11.029

Levy, M., L. Bopp, P. Karleskind, L. Resplandy, C. Ethe, and F. Pinsard. 2013. Physical pathways for carbon transfers between the surface mixed layer and the ocean interior. Global Biogeochem. Cycles **27**: 1001–1012. doi:10.1002/gbc.20092

Lomas, M. W., and S. B. Moran. 2011. Evidence for aggregation and export of cyanobacteria and nano-eukaryotes from the Sargasso Sea euphotic zone. Biogeosciences **8**: 203–216. doi:10.5194/bg-8-203-2011

Lombard, F., and T. Kiorboe. 2010. Marine snow originating from appendicularian houses: Age-dependent settling characteristics. Deep-Sea Res. Part I Oceanogr. Res. Pap. **57**: 1304–1313. doi:10.1016/j.dsr.2010.06.008

Lynn, R. J., and J. J. Simpson. 1987. The California Current System: The seasonal variability of its physical characteristics. J. Geophys. Res. Oceans **92**: 12947–12966. doi:10.1029/JC092iC12p12947

Maiti, K., C. R. Benitez-Nelson, M. W. Lomas, and J. W. Krause. 2009. Biogeochemical responses to late-winter storms in the Sargasso Sea, III-estimates of export production using Th-234:U-238 disequilibria and sediment traps. Deep-Sea Res. Part I Oceanogr. Res. Pap. **56**: 875–891. doi:10.1016/j.dsr.2009.01.008

Martin, J. H., G. A. Knauer, D. M. Karl, and W. W. Broenkow. 1987. Vertex: Carbon cycling in the northeast Pacific. Deep-Sea Res. Part A Oceanogr. Res. Pap. **34**: 267–285. doi:10.1016/0198-0149(87)90086-0

McDonnell, A. M. P., and K. O. Buesseler. 2010. Variability in the average sinking velocity of marine particles. Limnol. Oceanogr. **55**: 2085–2096. doi:10.4319/lo.2010.55.5.2085

McDonnell, A. M. P., P. W. Boyd, and K. O. Buesseler. 2015*a*. Effects of sinking velocities and microbial respiration rates on the attenuation of particulate carbon fluxes through the mesopelagic zone. Global Biogeochem. Cycles **29**: 175–193. doi:10.1002/2014GB004935

McDonnell, A. M. P., and others. 2015*b*. The oceanographic toolbox for the collection of sinking and suspended marine particles. Prog. Oceanogr. **133**: 17–31. doi:10.1016/j.pocean.2015.01.007

Miller, A. J., H. Song, and A. C. Subramanian. 2015. The physical oceanographic environment during the CCE-

LTER years: Changes in climate and concepts. Deep-Sea Res. Part II Top. Stud. Oceanogr. **112**: 6–17. doi:10.1016/j.dsr2.2014.01.003

Moore, A. M., H. G. Arango, G. Broquet, B. S. Powell, A. T. Weaver, and J. Zavala-Garay. 2011. The Regional Ocean Modeling System (ROMS) 4-dimensional variational data assimilation systems Part I - system overview and formulation. Prog. Oceanogr. **91**: 34–49. doi:10.1016/j.pocean.2011.05.004

Najjar, R. G., and others. 2007. Impact of circulation on export production, dissolved organic matter, and dissolved oxygen in the ocean: Results from Phase II of the Ocean Carbon-cycle Model Intercomparison Project (OCMIP-2). Global Biogeochem. Cycles **21**: 22. doi:10.1029/2006GB002857

North, E. W., R. R. Hood, S. Y. Chao, and L. P. Sanford. 2006. Using a random displacement model to simulate turbulent particle motion in a baroclinic frontal zone: A new implementation scheme and model performance tests. J. Mar. Syst. **60**: 365–380. doi:10.1016/j.jmarsys.2005.08.003

Ohman, M. D., K. Barbeau, P. J. S. Franks, R. Goericke, M. R. Landry, and A. J. Miller. 2013. Ecological transitions in a coastal upwelling ecosystem. Oceanography **26**: 210–219. doi:10.5670/oceanog.2013.65

Omand, M. M., E. A. D'Asaro, C. M. Lee, M. J. Perry, N. Briggs, I. Cetinić, and A. Mahadevan. 2015. Eddy-driven subduction exports particulate organic carbon from the spring bloom. Science **348**: 222–225. doi:10.1126/science.1260062

Picheral, M., L. Guidi, L. Stemmann, D. M. Karl, G. Iddaoud, and G. Gorsky. 2010. The Underwater Vision Profiler 5: An advanced instrument for high spatial resolution studies of particle size spectra and zooplankton. Limnol. Oceanogr.: Methods **8**: 462–473. doi:10.4319/lom.2010.8.462

Plattner, G. K., N. Gruber, H. Frenzel, and J. C. Mcwilliams. 2005. Decoupling marine export production from new production. Geophys. Res. Lett. **32**: 1–4. doi:10.1029/2005GL022660

Rodier, M., and R. Le Borgne. 1997. Export flux of particles at the equator in the western and central Pacific Ocean. Deep-Sea Res. Part II Top. Stud. Oceanogr. **44**: 2085–2113. doi:10.1016/S0967-0645(97)00092-1

Samo, T. J., and others. 2012. Microbial distribution and activity across a water mass frontal zone in the California Current Ecosystem. J. Plankton Res. **34**: 802–814. doi:10.1093/plankt/fbs048

Sarmiento, J. L., J. Dunne, A. Gnanadesikan, R. M. Key, K. Matsumoto, and R. Slater. 2002. A new estimate of the CaCO3 to organic carbon export ratio. Global Biogeochem. Cycles **16**. doi:10.1029/2002GB001919

Schlitzer, R. 2002. Carbon export fluxes in the Southern Ocean: Results from inverse modeling and comparison with satellite-based estimates. Deep-Sea Res. Part II Top.

Stud. Oceanogr. **49**: 1623–1644. doi:10.1016/S0967-0645(02)00004-8

Siegel, D. A., T. C. Granata, A. F. Michaels, and T. D. Dickey. 1990. Mesoscale eddy diffusion, particle sinking, and the interpretation of sediment trap data. J. Geophys. Res. Oceans **95**: 5305–5311. doi:10.1029/JC095iC04p05305

Siegel, D. A., and W. G. Deuser. 1997. Trajectories of sinking particles in the Sargasso Sea: Modeling of statistical funnels above deep-ocean sediment traps. Deep-Sea Res. Part I Oceanogr. Res. Pap. **44**: 1519–1541. doi:10.1016/S0967-0637(97)00028-9

Siegel, D. A., E. Fields, and K. O. Buesseler. 2008. A bottom-up view of the biological pump: Modeling source funnels above ocean sediment traps. Deep-Sea Res. Part I Oceanogr. Res. Pap. **55**: 108–127. doi:10.1016/j.dsr.2007.10.006

Smayda, T. J. 1971. Normal and accelerated sinking of phytoplankton in sea. Mar. Geol. **11**: 105–122. doi:10.1016/0025-3227(71)90070-3

Smayda, T. J., and P. K. Bienfang. 1983. Suspension properties of various phyletic groups of phytoplankton and tintinnids in an oligotrophic subtropical system. Mar. Ecol. **4**: 289–300. doi:10.1111/j.1439-0485.1983.tb00115.x

Sohrin, R., M. Isaji, Y. Obara, S. Agostini, Y. Suzuki, Y. Hiroe, T. Ichikawa, and K. Hidaka. 2011. Distribution of Synechococcus in the dark ocean. Aquat. Microb. Ecol. **64**: 1–14. doi:10.3354/ame01508

Song, H., A. J. Miller, S. Mcclatchie, E. D. Weber, K. M. Nieto, and D. M. Checkley. 2012. Application of a data-assimilation model to variability of Pacific sardine spawning and survivor habitats with ENSO in the California Current System. J. Geophys. Res. Oceans **117**: C03009. doi:10.1029/2011JC007302

Stanton, T. P., C. S. Law, and A. J. Watson. 1998. Physical evolution of the IronEx-I open ocean tracer patch. Deep-Sea Res. Part II Top. Stud. Oceanogr. **45**: 947–975. doi:10.1016/S0967-0645(98)00018-6

Steinberg, D. K., B. A. S. Van Mooy, K. O. Buesseler, P. W. Boyd, T. Kobari, and D. M. Karl. 2008. Bacterial vs. zooplankton control of sinking particle flux in the ocean's twilight zone. Limnol. Oceanogr. **53**: 1327–1338. doi:10.4319/lo.2008.53.4.1327

Stemmann, L., G. A. Jackson, and D. Ianson. 2004. A vertical model of particle size distributions and fluxes in the midwater column that includes biological and physical processes-part I: Model formulation. Deep-Sea Res. Part I Oceanogr. Res. Pap. **51**: 865–884. doi:10.1016/j.dsr.2004.03.001

Stukel, M. R., and M. R. Landry. 2010. Contribution of picophytoplankton to carbon export in the equatorial Pacific: A re-assessment of food-web flux inferences from inverse models. Limnol. Oceanogr. **55**: 2669–2685. doi:10.4319/lo.2010.55.6.2669

Stukel, M. R., M. R. Landry, C. R. Benitez-Nelson, and R. Goericke. 2011. Trophic cycling and carbon export relationships in the California Current Ecosystem. Limnol. Oceanogr. **56**: 1866–1878. doi:10.4319/lo.2011.56.5.1866

Stukel, M. R., M. R. Landry, M. D. Ohman, R. Goericke, T. Samo, and C. R. Benitez-Nelson. 2012. Do inverse ecosystem models accurately reconstruct plankton trophic flows? Comparing two solution methods using field data from the California Current. J. Mar. Syst. **91**: 20–33. doi:10.1016/j.jmarsys.2011.09.004

Stukel, M. R., M. D. Ohman, C. R. Benitez-Nelson, and M. R. Landry. 2013. Contributions of mesozooplankton to vertical carbon export in a coastal upwelling system. Mar. Ecol. Prog. Ser. **491**: 47–65. doi:10.3354/meps10453

Stukel, M. R., K. A. S. Mislan, M. Décima, and L. Hmelo. 2014. Detritus in the pelagic ocean. *In* P. F. Kemp [ed.], Eco-DAS IX Symposium Proceedings. Association for the Sciences of Limnology and Oceanography. 49–76.

Stukel, M. R., E. Asher, N. Couto, O. Schofield, S. Strebel, P. Tortell, and H. W. Ducklow. 2015. The imbalance of new and export production in the western Antarctic Peninsula, a potentially "leaky" ecosystem. Global Biogeochem. Cycles **29**: 1400–1420. doi:10.1002/2015GB005211

Stukel, M. R., and others. 2017. Mesoscale ocean fronts enhance carbon export due to gravitational sinking and subduction. Proc. Natl. Acad. Sci. USA. **114**: 1252–1257. doi:10.1073/pnas.1609435114

Takahashi, T., W. S. Broecker, and S. Langer. 1985. Redfield ratio based on chemical data from isopycnal surfaces. J. Geophys. Res. Oceans **90**: 6907–6924. doi:10.1029/JC090iC04p06907

Trull, T. W., S. G. Bray, K. O. Buesseler, C. H. Lamborg, S. Manganini, C. Moy, and J. Valdes. 2008. In situ measurement of mesopelagic particle sinking rates and the control of carbon transfer to the ocean interior during the Vertical Flux in the Global Ocean (VERTIGO) voyages in the North Pacific. Deep-Sea Res. Part II Top. Stud. Oceanogr. **55**: 1684–1695. doi:10.1016/j.dsr2.2008.04.021

Turner, J. T. 2002. Zooplankton fecal pellets, marine snow and sinking phytoplankton blooms. Aquat. Microb. Ecol. **27**: 57–102. doi:10.3354/ame027057

Turner, J. T. 2015. Zooplankton fecal pellets, marine snow, phytodetritus and the ocean's biological pump. Prog. Oceanogr. **130**: 205–248. doi:10.1016/j.pocean.2014.08.005

Venrick, E. L. 1998. Spring in the California current: The distribution of phytoplankton species, April 1993 and April 1995. Mar. Ecol. Prog. Ser. **167**: 73–88. doi:10.3354/meps167073

Volk, T., and M. I. Hoffert. 1985. Ocean carbon pumps: Analysis of relative strengths and efficiencies in ocean-driven atmospheric CO2 changes, p. 99–110. In E. T. Sundquist and W. S. Broeker [eds.], The carbon cycle and atmospheric CO2: Natural variations archean to present. American Geophysical Union.

Waite, A. M., K. A. Safi, J. A. Hall, and S. D. Nodder. 2000. Mass sedimentation of picoplankton embedded in organic

aggregates. Limnol. Oceanogr. **45**: 87–97. doi:10.4319/lo.2000.45.1.0087

Wilson, S. E., D. K. Steinberg, and K. O. Buesseler. 2008. Changes in fecal pellet characteristics with depth as indicators of zooplankton repackaging of particles in the mesopelagic zone of the subtropical and subarctic North Pacific Ocean. Deep-Sea Res. Part II Top. Stud. Oceanogr. **55**: 1636–1647. doi:10.1016/j.dsr2.2008.04.019

Conflict of Interest

None declared.